

Atmos. Chem. Phys., 15, 11477–11499, 2015  
www.atmos-chem-phys.net/15/11477/2015/  
doi:10.5194/acp-15-11477-2015  
© Author(s) 2015. CC Attribution 3.0 License.

Atmospheric  
Chemistry  
and Physics  
Open Access



# Transport pathways of peroxyacetyl nitrate in the upper troposphere and lower stratosphere from different monsoon systems during the summer monsoon season

S. Fadnavis<sup>1</sup>, K. Semeniuk<sup>2</sup>, M. G. Schultz<sup>3</sup>, M. Kiefer<sup>4</sup>, A. Mahajan<sup>1</sup>, L. Pozzoli<sup>5</sup>, and S. Sonbawane<sup>1</sup>

<sup>1</sup>Indian Institute of Tropical Meteorology, Pune, India

<sup>2</sup>Department of Earth and Space Sciences and Engineering, York University, Toronto, Canada

<sup>3</sup>Institute for Energy and Climate Research-Troposphere (IEK-8), Forschungszentrum Jülich, Jülich, Germany

<sup>4</sup>Karlsruhe Institute of Technology, Institute for Meteorology and Climate Research, Karlsruhe, Germany

<sup>5</sup>Eurasia Institute of Earth Sciences, Istanbul Technical University, Istanbul, Turkey

Correspondence to: S. Fadnavis ([suvarna@tropmet.res.in](mailto:suvarna@tropmet.res.in))

Received: 17 April 2015 – Published in Atmos. Chem. Phys. Discuss.: 1 June 2015

Revised: 2 October 2015 – Accepted: 2 October 2015 – Published: 19 October 2015

**Abstract.** The Asian summer monsoon involves complex transport patterns with large-scale redistribution of trace gases in the upper troposphere and lower stratosphere (UTLS). We employ the global chemistry–climate model ECHAM5–HAMMOZ in order to evaluate the transport pathways and the contributions of nitrogen oxide species peroxyacetyl nitrate (PAN), NO<sub>x</sub> and HNO<sub>3</sub> from various monsoon regions, to the UTLS over southern Asia and vice versa. Simulated long-term seasonal mean mixing ratios are compared with trace gas retrievals from the Michelson Interferometer for Passive Atmospheric Sounding aboard ENVISAT(MIPAS-E) and aircraft campaigns during the monsoon season (June–September) in order to evaluate the model's ability to reproduce these transport patterns.

The model simulations show that there are three regions which contribute substantial pollution to the South Asian UTLS: the Asian summer monsoon (ASM), the North American monsoon (NAM) and the West African monsoon (WAM). However, penetration due to ASM convection reaches deeper into the UTLS compared to NAM and WAM outflow. The circulation in all three monsoon regions distributes PAN into the tropical latitude belt in the upper troposphere (UT). Remote transport also occurs in the extratropical UT where westerly winds drive North American and European pollutants eastward where they can become part of the ASM convection and lifted into the lower stratosphere. In the lower stratosphere the injected pollutants are trans-

ported westward by easterly winds. Sensitivity experiments with ECHAM5–HAMMOZ for simultaneous NO<sub>x</sub> and non-methane volatile organic compounds (NMVOCs) emission change (–10 %) over ASM, NAM and WAM confirm similar transport. Our analysis shows that a 10 % change in Asian emissions transports ~5–30 ppt of PAN in the UTLS over Asia, ~1–10 ppt of PAN in the UTLS of northern subtropics and mid-latitudes, ~7–10 ppt of HNO<sub>3</sub> and ~1–2 ppb of ozone in UT over Asia. Comparison of emission change over Asia, North America and Africa shows that the highest transport of HNO<sub>3</sub> and ozone occurs in the UT over Asia and least over Africa.

The intense convective activity in the monsoon regions is associated with lightning and thereby the formation of additional NO<sub>x</sub>. This also affects the distribution of PAN in the UTLS. Simulations with and without lightning show an increase in the concentrations of PAN (~40 %), HNO<sub>3</sub> (75%), NO<sub>x</sub> (70 %) and ozone (30 %) over the regions of convective transport. Lightning-induced production of these species is higher over equatorial Africa and America compared to the ASM region. This indicates that the contribution of anthropogenic emissions to PAN in the UTLS over the ASM is higher than that of lightning.

## 1 Introduction

Deep monsoon convection plays a key role in venting chemical constituents from the boundary layer and their export from source regions (Dickerson et al., 1987). The largest regional monsoon systems are the North American monsoon (NAM), Asian summer monsoon (ASM), western North Pacific monsoon (WNPM), South American monsoon (SAM), West African monsoon (WAM) and the Australian monsoon (AUSM) (Chang et al., 2011). Recent observation and modeling studies indicate that the Asian summer monsoon (Park et al., 2004, 2007; Li et al., 2005; Randel and Park, 2006; Fu et al., 2006; Xiong et al., 2009; Randel et al., 2010; Fadnavis et al., 2013), the North American monsoon (Schmitz and Mullen 1996; Collier and Zhang, 2006; Barth et al., 2012) and the West African monsoon (Bouarar et al., 2011) play important roles in the transport of chemical constituents out of the boundary layer into the Northern Hemisphere in the upper troposphere (UT). A number of studies have documented that large amounts of pollution from Asia are transported across the tropopause (Park et al., 2007; Fu et al., 2006); however, transport from other monsoon systems (WAM, NAM) and their contribution to Asia have so far received less attention. Until now there has been no attempt to assess the relative contributions from these source regions and to analyze the transport patterns including possible recirculation within one consistent model framework. Prior model simulations suggest that pollutants transported from the Asian monsoon region can contribute substantially to the budgets of stratospheric ozone,  $\text{NO}_x$  and water vapor (Randel et al., 2010). Ozone formation in the anticyclone is also enhanced by transport of pollution plumes from the North American monsoon which are rich in volatile organic compounds (VOCs) (Li et al., 2005; Zhang et al., 2008; Choi et al., 2009; Barth et al., 2012). The deep monsoon convection over West Africa transports central African emissions to the upper troposphere and lower stratosphere (UTLS), leading to large ozone changes in the lower stratosphere (Bouarar et al., 2011). A number of studies have reported transport of chemical constituents into the UTLS due to the Asian monsoon convection, while less attention has been paid to deep convective transport from North/South America and West Africa to the lower stratosphere and to their relative contributions to the UTLS composition over the ASM region.

This study investigates the transport patterns and relative contributions to the Asian monsoon anticyclone of three oxidized nitrogen species, namely peroxyacetyl nitrate (PAN),  $\text{NO}_x$  (the sum of  $\text{NO}$  and  $\text{NO}_2$ ) and nitric acid ( $\text{HNO}_3$ ). PAN is a secondary pollutant that marks the transport and conversion of surface  $\text{NO}_x$  after it is emitted. The focus of this study is placed on PAN as this species has a long lifetime (90–180 days) in the UT and can be favorably observed by satellite instruments. At the same time, its short chemical lifetime in the lower troposphere (not longer than 30 days) results in a much tighter association between the emissions

regions of its precursors and transport compared to species such as carbon monoxide (CO). The much longer chemical lifetime of CO in the lower troposphere allows it to reach the UTLS via circuitous pathways that are not accessible to PAN. In contrast, PAN is a tracer that allows for a clearer identification of  $\text{NO}_x$  pollution transport pathways between the surface and the UTLS. We perform  $\text{NO}_x$  and NMVOCs (non-methane volatile organic compounds) emission sensitivity simulations (where emissions of  $\text{NO}_x$  and NMVOCs were simultaneously reduced by 10 %) in order to investigate the relative contributions from Asia, Africa and America to the PAN,  $\text{HNO}_3$  and  $\text{O}_3$  concentrations in the UTLS.

PAN is formed through the oxidation of NMVOCs in the presence of  $\text{NO}_x$  (Fischer et al., 2014). It is primarily formed after oxidation of acetaldehyde ( $\text{CH}_3\text{CHO}$ ) or after photolysis of acetone ( $\text{CH}_3\text{COCH}_3$ ) and methyl glyoxal ( $\text{CH}_3\text{COCHO}$ ), all of which are oxidation products of various NMVOCs. The actual formation of PAN proceeds in the reaction of the peroxy acetyl radical ( $\text{CH}_3\text{CO}_3$ ) with  $\text{NO}_2$ . This reaction is reversible and the thermal decomposition of PAN back to  $\text{CH}_3\text{CO}_3$  and  $\text{NO}_2$  is the main sink of PAN, although in the UTLS, PAN photolysis becomes the dominant loss process. Two minor loss processes of PAN are reactions with OH and dry deposition (Talukdar et al., 1995; Fischer et al., 2014). As stated by Fischer et al. (2014) global, biogenic VOCs like isoprene and terpenes, contribute most to PAN formation, but in the context of our study it is important to note that the oxidation of many alkanes and alkenes which are emitted from anthropogenic sources lead to PAN formation as well. The major anthropogenic sources of NMVOCs are the emissions from fossil fuel and biofuel combustion and from industrial solvents (Tang et al., 2009). Biomass burning, biogenic and soil emissions also contribute to NMVOC and  $\text{NO}_x$  production. Anthropogenic sources are dominant in the extratropical Northern Hemisphere outside the spring season. In spring, when surface PAN peaks, biogenic and anthropogenic NMVOCs species are responsible for  $\sim 50\%$  of the PAN burden.

In the UT, lightning can add substantial amounts of  $\text{NO}_x$  and thus lead to additional PAN production if NMVOC precursors are present, e.g., from convective uplifting from the boundary layer (Tie et al., 2001). The estimated global  $\text{NO}_x$  production by lightning is  $\sim 3\text{--}5\text{ Tg N year}^{-1}$  (Schumann and Huntrieser, 2007; Martin et al., 2007; Murray et al., 2012). Strong lightning activity during ASM, NAM and WAM (Shepon, et al., 2007; Evett et al., 2008; Ranalkar and Chaudhari, 2009; Barret et al., 2010; Penki and Kamra, 2013) hence contributes to PAN production in the UTLS. The estimated increase in PAN is  $\sim 20\text{--}30\%$  due to  $\text{NO}_x$  enhancement by lightning (Tie et al., 2001).

The thermal decomposition rate of PAN is highly temperature-dependent. In the UTLS, temperatures are sufficiently low to prevent thermal decomposition of PAN and therefore the chemical lifetime of PAN in this region is  $\sim 90\text{--}180$  days (Arnold and Hauck, 1985). The PAN lifetime

in our ECHAM5–HAMMOZ simulations varies between 80 days and 170 days in the tropical UTLS. Several studies (Tereszchuk et al., 2013; Glatthor et al., 2007; Singh et al., 1987) have reported that the lifetime of PAN varies between 2 and 4 months. PAN thus travels over long distances and affects the  $\text{NO}_y$  partitioning in areas that are far away from the precursor emission regions. Upon descent into warmer regions of the troposphere, PAN releases  $\text{NO}_x$  which in turn increases ozone and OH production in remote regions (Singh et al., 1986, 1998; Hudman et al., 2004). PAN mixing ratios vary from less than 1 pptv in the remote marine atmosphere (as observed during the NASA GTE PEM-Tropics B campaign in the South Pacific lower marine boundary layer, data available at <http://acd.ucar.edu/~emmons/DATACOMP/>) to several parts per billion by volume in the polluted urban environment and biomass burning plumes (Ridley et al., 1992; Singh et al., 1998). In the UTLS, mixing ratios are typically in the range 10–300 pptv (Emmons et al., 2000; Keim et al., 2008).

To our knowledge, our study is the first study that analyzes the influence of monsoon outflow from different world regions on the distribution of peroxyacetyl nitrate (PAN) in the UTLS over the Asian monsoon region, and its recirculation in the UTLS. We run decadal simulations with the chemistry–climate model ECHAM5–HAMMOZ. In emission sensitivity experiments,  $\text{NO}_x$  and NMVOCs emissions were simultaneously reduced by 10 % over ASM, WAM and NAM to understand regional contribution. We apply statistical comparisons with satellite and aircraft data, thereby contributing to the objectives of the Chemistry–Climate Model Initiative (CCMI, see <http://www.igacproject.org/CCMI>). The model climatology is evaluated with data from aircraft campaigns and the Michelson Interferometer for Passive Atmospheric Sounding (MIPAS) instrument on-board the ENVIRONMENTAL SATellite (ENVISAT) (referred to as MIPAS-E hereafter). The transport of  $\text{HNO}_3$  and  $\text{NO}_x$  due to monsoon convection from different monsoon regions and the impacts of lightning on the UTLS distributions of nitrogen oxide are also analyzed and compared to the results obtained for PAN. The paper is organized as follows: Sect. 2 contains a short description of the data and model including the simulation setup. Comparisons of model simulations with observations are given in Sect. 3. In Sect. 4, we discuss the various convective transport pathways of PAN into the UTLS, its redistribution in the stratosphere and its recirculation across the various monsoon regions as well as results of the emission sensitivity simulations depicting the contributions from major monsoon systems. The analysis of percentage changes in lightning-produced ozone,  $\text{HNO}_3$ , PAN and  $\text{NO}_x$  on total concentrations over the convective zones is presented in Sect. 5. Conclusions are given in Sect. 6.

## 2 Methods

### 2.1 Satellite measurements

MIPAS-E instrument was launched in March 2002 into a polar orbit of 800 km altitude, with an orbital period of about 100 min and an orbit repeat cycle of 35 days. MIPAS-E (Fischer and Oelhaf, 1996; Fischer et al., 2008) was a Fourier transform spectrometer that provided continual limb emission measurements in the mid-infrared over the range 685–2410  $\text{cm}^{-1}$  (14.6–4.15  $\mu\text{m}$ ). From January 2005 through the end of the mission in April 2012, MIPAS-E was operated with a spectral resolution of 0.0875  $\text{cm}^{-1}$ , and a stepping of the tangent altitude of 1.5–2 km in the UTLS region. As a mid-infrared sounder, MIPAS-E could not provide spectral information from below the cloud top.

MIPAS-E monitored several atmospheric trace constituents affecting atmospheric chemistry including PAN,  $\text{NO}_x$  and  $\text{O}_3$ . The details of the general retrieval method and setup, error estimates and use of averaging kernel and visibility flag are documented by von Clarmann et al. (2009). In this study we analyze the MIPAS-E observed PAN data during the period 2005–2012, i.e., the data version V5R\_PAN\_220/V5R\_PAN\_221 (different naming 220/221 merely due to technical reasons). The data are available from [http://share.lsd.kit.edu/imk/asf/sat/kiefer/To\\_Richard/](http://share.lsd.kit.edu/imk/asf/sat/kiefer/To_Richard/). Details of the MIPAS-E PAN retrievals, error budget and vertical resolution are given by Glatthor et al. (2007) and by Wiegeler et al. (2012). Table 3 in Wiegeler et al. (2012) indicates that for the total error of single profiles of the V5R\_PAN\_220/221 product, the spectral noise and the uncertainty of the instrument pointing are the main contributors. However, since noise is a major contributor a reduction of the total error can be expected for vertical profiles of binned data. For typical bins used in this work the total errors are less than 10 % below 12 km, 30 % at 15 km, 50 % at 19 km and 80 % at 23 km.

The sensitivity of the PAN retrievals can be judged by the averaging kernels. For the V5R\_PAN\_220/221 product an example of the respective averaging kernel rows is shown in Fig. S1 in the Supplement for an altitude range of 5 to 25 km at 28° N and 85° E for cloud-free atmospheric conditions. The diamonds indicate the respective nominal altitudes of the retrieval grid. The figure shows that the retrieval results below 8–9 km are dominated by information from above the nominal altitude. A similar, albeit less obvious, situation develops for altitudes above 22–23 km. There and above, the information has an increasing weight from lower than nominal altitudes. This is the reason why the MIPAS-E PAN data are not considered below 8 km and above 23 km. Another effect clearly visible in the example is that the altitude region which influences the retrieved PAN value at a given altitude increases with altitude, i.e., the vertical resolution decreases with altitude. To account for the comparatively low, and altitude-dependent, vertical resolution, the model data to

be directly compared to MIPAS-E measurements were convolved with the MIPAS-E PAN averaging kernel.

The data are contoured and gridded at 4° latitude and 8° longitude resolution. In the process the data quality specifications as documented at <http://share.lsd.fkit.edu/imk/asf/sat/mipas-export/Documentation/> were employed, namely: only data with a visibility flag equal to 1 and a diagonal value of averaging kernel greater than 0.03 were used.

## 2.2 ECHAM5–HAMMOZ model simulation and experimental setup

The ECHAM5–HAMMOZ aerosol-chemistry–climate model used in the present study is comprised of the general circulation model ECHAM5 (Roeckner et al., 2003), the tropospheric chemistry module, MOZ (Horowitz et al., 2003), and the aerosol module, Hamburg Aerosol Model (HAM) (Stier et al., 2005). It includes ozone, NO<sub>x</sub>, VOC and aerosol chemistry. The gas-phase chemistry scheme is based on the MOZART-2 model (Horowitz et al., 2003), which includes comprehensive O<sub>x</sub>–NO<sub>x</sub>–hydrocarbons chemistry with 63 tracers and 168 reactions. The O(<sup>1</sup>D) quenching reaction rates were updated according to Sander et al. (2003) and isoprene nitrates chemistry according to Fiore et al. (2005). In the model simulations we included emissions of acetone from anthropogenic sources and wild fires (primary sources), while acetaldehyde and methylglyoxal are produced by oxidation of other NMVOCs (secondary sources). In particular, oxidation of primary NMVOCs like ethane (C<sub>2</sub>H<sub>6</sub>), propane (C<sub>3</sub>H<sub>8</sub>) and propene (C<sub>3</sub>H<sub>6</sub>) forms acetaldehyde, while CH<sub>3</sub>COCHO is mainly formed from the oxidation products of isoprene and terpenes. Higher acyl peroxy nitrates (MPAN) have been included in the MOZART-2 chemical scheme, which are also formed through oxidation of NMVOCs, but their production is small compared to PAN. Thermal decomposition, and reaction with OH as well as the absorption cross sections for PAN photolysis are all specified according to Sander et al. (2003).

In ECHAM5–HAMMOZ dry deposition follows the scheme of Ganzeveld and Lelieveld (1995). Soluble trace gases such as HNO<sub>3</sub> and SO<sub>2</sub> are also subject to wet deposition. In-cloud and below-cloud scavenging follows the scheme described by Stier et al. (2005). PAN is not water-soluble, therefore dry and wet deposition are insignificant removal processes.

The model is run at a spectral resolution of T42 corresponding to about 2.8 × 2.8° in the horizontal dimension and 31 vertical hybrid  $\sigma$ -p levels from the surface up to 10 hPa. We note that the nominal grid resolution of 2.8° is somewhat misleading, because the spectral truncation of T42 only allows to resolve details on the order of 180/42 = 4.28°. This is the main reason why we compare our model results with the MIPAS-E PAN retrievals on a 4 × 8° grid. The details of model parameterizations, emissions and validation are de-

scribed by Pozzoli et al. (2008a, b, 2011) and Fadnavis et al. (2013).

The model simulations were performed with varying monthly mean sea surface temperature (SST) and sea ice cover (SIC) data over the period 2000–2010 (AMIP) referred to as the control simulation. The simulations did not aim to exactly reproduce specific meteorological years, and we ran 11-year periods in order to obtain reasonable statistics. We used the RETRO project data set of the year 2000 available at <http://eccad.sedoo.fr/> for the surface CO, NO<sub>x</sub> and hydrocarbon emissions from anthropogenic sources and biomass burning (Schultz et al., 2007, 2008). Anthropogenic total RETRO emissions of the year 2000 are 476 Tg year<sup>-1</sup> for CO, 90 Tg year<sup>-1</sup> for NO<sub>x</sub>, 5 Tg year<sup>-1</sup> of ethane, 3.5 Tg year<sup>-1</sup> of propane and 2.7 Tg year<sup>-1</sup> of propene, which are the main anthropogenic VOC precursors of PAN. Biomass burning RETRO emissions of year 2000 are 357 Tg year<sup>-1</sup> for CO, 16 Tg year<sup>-1</sup> for NO<sub>x</sub>, 2.5 Tg year<sup>-1</sup> for ethane, 1.3 Tg year<sup>-1</sup> for propane, 2.7 Tg year<sup>-1</sup> for propene and 2.7 Tg year<sup>-1</sup> for acetone. CO biomass burning emissions in Southeast Asia account for 7 Gg month<sup>-1</sup> in spring, while up to 15 Gg month<sup>-1</sup> were reported from Carmichael et al. (2003). The anthropogenic and biomass burning emissions of SO<sub>2</sub> (total of 142 Tg year<sup>-1</sup>), BC (7.7 Tg year<sup>-1</sup>) and OC (66.1 Tg year<sup>-1</sup>) are based on the AEROCOM emission inventory (Dentener et al., 2006), also representative of the year 2000. The biogenic NMVOC emissions are calculated online with the MEGAN module of Guenther et al. (2006). The simulated global annual mean emission of biogenic NMVOCs between 1995 and 2004 is 830 Tg(C) year<sup>-1</sup>; isoprene contributes 57 %, followed by terpenes (21 %), methanol (12 %) and other NMVOCs such as acetaldehyde (2.5 %) and acetone (2.3 %). Other natural emissions calculated online by the model are the dimethyl sulfide (DMS) fluxes (Kettle and Andreae, 2000; Nightingale et al., 2000; Pham et al., 1995), sea salt aerosols (Schulz et al., 2004) from the ocean and mineral dust aerosols (Tegen et al., 2002; Cheng et al., 2008).

Our base year for aerosol and trace gas emissions is 2000, and emissions were repeated annually throughout the simulation period. One point to note is that there were substantial emission changes in Asia and Africa (increasing trends) and Europe and North America (decreasing trends) during the study period, which are not captured in our simulations. A consequence of these emission changes for our study would be that we may underestimate the impact of local pollution sources on PAN concentrations in the UTLS over the ASM region in recent years and that we overestimate the contribution from long-range transport of northern hemispheric pollution. We provide an estimate of this error in the discussion of the results. Lightning NO<sub>x</sub> emissions are parameterized following Grewe et al. (2001). They are proportional to the calculated flash frequency with a production rate of 9 kg(N) per flash, and distributed vertically using a C-shaped profile. The calculated flash frequency is resolution-dependent and

scaled globally to yield annual global emissions of 3.4 Tg(N) per year. To study the impact of lightning on the distributions of PAN we compare two sets of experiments; each were conducted for 11 years, 2000–2010: (1) the control experiment (CTRL) and (2) the lightning-off experiment (light-off).

Model-simulated PAN, NO<sub>x</sub>, HNO<sub>3</sub> and O<sub>3</sub> mixing ratios are evaluated with climatological data sets of airborne campaigns during the monsoon season (June–September). The data were retrieved from <http://acd.ucar.edu/~emmons/DATACOMP/CAMPAIGNS/> (see also the paper by Emmons, 2001). The NO<sub>x</sub> and ozone volume mixing ratios observed during Cloud Aerosol Interaction and Precipitation Enhancement Experiment (CAIPEEX) (details available in Kulkarni et al., 2012), September 2010, are evaluated over the Indian region. The details of instruments and measurement techniques are available at <http://www.tropmet.res.in/~caipeex/about-data.php>. The list of data sets and aircraft campaign used for comparison are presented in Table 1. For the comparison, aircraft observations are averaged over 0–2, 2–6 and 6–8 km and horizontally over the coherent flight regions.

In order to understand the impact of NO<sub>x</sub> and NMVOCs emissions on the distribution of PAN, we conducted a reference run and three emission sensitivity simulations for the year 2003 driven by European Centre for Medium-Range Weather Forecasts operational analyses (Integrated Forecast System (IFS) cycle-32r2) meteorological fields (available every 6 h) (Uppala et al., 2005). Model simulations were performed for the year 2003 since there was no significant oceanic/meteorological perturbation event like, e.g., El Niño–Southern Oscillation or the Indian Ocean Dipole ([http://www.marine.csiro.au/~mcintosh/Research\\_ENSO\\_IOD\\_years.htm](http://www.marine.csiro.au/~mcintosh/Research_ENSO_IOD_years.htm)). In experiments 1 to 3, emissions of both NO<sub>x</sub> and MNVOCs were simultaneously reduced by 10 % over (1) Asia (10° S–50° N, 60–130° E), (2) Africa (30° S–30° N, 15° W–45° E) and (3) North America (15–45° N, 120–75° W), referred to separately as Asia–10 %, Africa–10 % and North America–10 %.

### 2.3 Model production of PAN

PAN is a secondary pollutant that has a short lifetime in the lower troposphere. This reduces the number of source points that contribute to PAN concentrations at any location in the UTLS, resulting in a clearer identification of source-receptor pathways. Figure 1 shows the distribution of PAN production at 14 and 16 km. A striking feature is the confinement of PAN production to regions of deep convection. A maximum daily production rate of PAN in the UTLS, in these convective zones, is > 24 ppt day<sup>-1</sup> near 14 km and > 12 ppt day<sup>-1</sup> near 16 km. Production of PAN from background concentrations of ethane (C<sub>2</sub>H<sub>6</sub>) and other NMVOCs outside of deep convection regions is distinctly secondary. NMVOCs are subject to the same convective transport as NO<sub>x</sub> and PAN formation

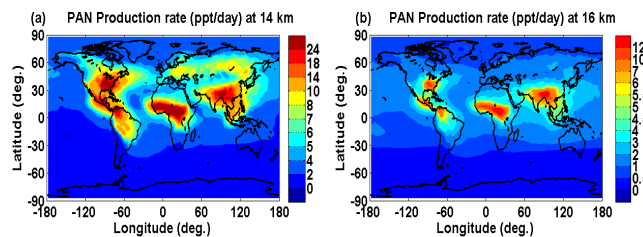


**Figure 1.** PAN production rates at (a) 14 km and (b) 16 km. Key regions of biomass burning and anthropogenic emissions of pollutants are evident and correspond to maxima in PAN production. Weaker dispersed background formation is evident as well.

occurs where both have the highest values. The lifetime of NO<sub>x</sub> is short throughout the troposphere which implies that PAN production in the UT can be associated with deep convection. There is also a contribution to PAN production from stratospheric air penetrating into the troposphere (Liang et al., 2011). Tropopause folding is a significant source of exchange between the stratosphere and the troposphere (Gettelman et al., 2011). This is an extratropical process that likely contributes to the PAN formation maxima over North America, Europe and Asia (shown in Fig. 1a) via enhanced conversion of ethane. In the model it is not possible to obscure the relationship between PAN formation and NO<sub>x</sub> pollution source regions.

## 3 Comparison of model simulations with observations

### 3.1 Comparison with aircraft measurements

Figure 2 shows scatter plots between aircraft observations and model simulations at the coherent locations. Both aircraft observations and model simulations are averaged for the monsoon season and altitude ranges. It indicates that model-simulated PAN, O<sub>3</sub> and NO<sub>x</sub> show good agreement with aircraft measurements; correlation coefficient > 0.7 and significance (*P* value) varies between 0.00 and 0.3, indicating that correlation is significant at 95 % confidence level; however, simulated HNO<sub>3</sub>, between 2 and 6 km, and 6 and 10 km, does not agree well with aircraft observations.

A point-to-point comparison of (latitude–longitude transects at various altitudes) simulated PAN, NO<sub>x</sub>, O<sub>3</sub> and HNO<sub>3</sub> (for the period 1995–2005) with aircraft observations are presented by Fadnavis et al. (2014). These plots show good agreement between model simulations and aircraft observations. Vertical variation of simulated ozone also shows good agreement with ozonesonde measurements over India (see Fig. S3 in the Supplement in Fadnavis 2014). It should be noted that current model simulations (2000–2010) show better agreement with aircraft observations than Fadnavis et al. (2014). Figures showing the difference between these simulations and the aircraft observations are provided in the

**Table 1.** Global aircraft measurements used for model evaluation.

Experiment	Time frame	Species	Location
POLINAT-2 (Falcon), Ziereis et al. (2000)	19 Sep–25 Oct 1997	O <sub>3</sub> , NO <sub>x</sub>	Canary Islands: LAT = 25, 35° N, LONG = 160, 170° W, East Atlantic: LAT = 35, 45° N, LONG = 150, 160° W, Europe: LAT = 45, 55° N, LONG = 5, 15° E, Ireland: LAT = 50, 60° N, LONG = 165, 175° W
PEM-Tropics A (DC8), Talbot et al. (2000)	24 Aug–15 Oct 1996	O <sub>3</sub> , NO <sub>x</sub> , HNO <sub>3</sub> , PAN	Christmas Island: LAT = 0, 10° N, LONG = 20, 40° W, Easter Island: LAT = −40° N, 20° S, LONG = 60, 80° W, Fiji: LAT = 0°, 10° S, LONG = 170° E, 10° W, Hawaii: LAT = 10, 30° N, LONG = 10, 30° W, Tahiti: LAT = 20° S, 0°, LONG = 20, 50° W
PEM-Tropics A (P3), O’Sullivan et al. (1999)	15 Aug–26 Sep 1996	O <sub>3</sub> , HNO <sub>3</sub>	Christmas Island: LAT = 0°, 10° N, LONG = 20, 40° W, Easter Island: LAT = 40, 20° S, LONG = 60, 80° W, Hawaii: LAT = 10, 30° N, LONG = 10, 30° W, Tahiti: LAT = 20° S, 0°, LONG = 20, 50° W
ABLE-3B (Electra), Harriss et al. (1994)	6 Jul–15 Aug 1990	O <sub>3</sub> , NO <sub>x</sub> , HNO <sub>3</sub> , PAN	Labrador: LAT = 50, 55° N, LONG = 120, 135° W, Ontario: LAT = 45, 60° N, LONG = 90, 100° W, US east coast: LAT = 35, 45° N, LONG = 100, 110° W
CITE-3 (Electra), Hoell et al. (1993)	22 Aug–29 Sep 1989	O <sub>3</sub> , NO <sub>x</sub>	Natal: LAT = 15° S, 5° N, LONG = 145, 155° W, Wallops: LAT = 30, 40° N, LONG = 100, 110° W
ELCHEM (Sabreliner), Ridley et al. (1994)	27 Jul–22 Aug 1989	O <sub>3</sub> , NO <sub>x</sub>	New Mexico: LAT = 30, 35° N, LONG = 70, 75° W
ABLE-3A (Electra), Harriss et al. (1992)	7 Jul–17 Aug 1988	O <sub>3</sub> , NO <sub>x</sub> , PAN	Alaska: LAT = 55, 75° N, LONG = 10, 25° W
ABLE-2A (Electra), Harriss et al. (1988)	12 Jul–13 Aug 1985	O <sub>3</sub>	East Brazil: LAT = 10° S, 0°, LONG = 120, 135° W, West Brazil: LAT = 5° S, 0°, LONG = 110, 120° W
STRAT0Z-3 (Caravelle 116), Drummond et al. (1988)	4–26 Jun 1984	O <sub>3</sub>	Brazil: LAT = 20° S, 0°, LONG = 135, 155° W, Canary Islands: LAT = 20, 35° N, LONG = 160, 155° W, E tropical North Atlantic: LAT = 0°, 20° N, LONG = 150, 165° W, England: LAT = 45, 60° N, LONG = 10° E, 5° W, Goose Bay: LAT = 45, 60° N, LONG = 110, 125° W, Greenland: LAT = 60, 70° N, LONG = 110, 150° W, Iceland: LAT = 60, 70° N, LONG = 150, 155° W, NW South America: LAT = −5, 10° N, LONG = 95, 115° W, Puerto Rico: LAT = 10, 25° N, LONG = 110, 120° W, S South America: LAT = 65, 45° S, LONG = 95, 120° W, SE South America: LAT = 45, 20° S, LONG = 115, 140° W, SW South America: LAT = −45, 25° S, LONG = 105, 112° W, Spain: LAT = 35, 45° N, LONG = 15° W, 0°, W Africa: LAT = 0°, 15° N, LONG = 15° W, 0°, W South America: LAT = 25, 5° S, LONG = 95, 110° W, Western North Atlantic: LAT = 25, 45° N, LONG = 110, 120° W
CITE-2 (Electra), Hoell et al. (1990)	11 Aug–5 Sep 1986	O <sub>3</sub> , NO <sub>x</sub> , HNO <sub>3</sub> , PAN	California: LAT = 35, 45° N, LONG = 55, 70° W, Pacific: LAT = 30, 45° N, LONG = 45, 55° W
INTEX-A, Singh et al. (2006)	Jul–Aug 2004	O <sub>3</sub> , PAN, NO <sub>x</sub>	Eastern North America: LAT = 29, 51° N, LONG: 44– 120° W
CAIPEEX, Prabha et al. (2011)	Sep–Oct 2010	O <sub>3</sub> , NO <sub>x</sub>	LAT = 12, 22° N, LONG = 74, 78° E

Supplement as Fig. S2. The model bias varies with species and altitude. In general, the bias in PAN ranges from −20 ppt to 80 ppt, for ozone from −2 to 40 ppb and for HNO<sub>3</sub> from −20 to 75 ppt, while NO<sub>x</sub> mixing ratios show a good agreement with CAIPEEX measurements over the Indian region.

Unfortunately, there were no measurements of PAN or HNO<sub>3</sub> made during CAIPEEX.

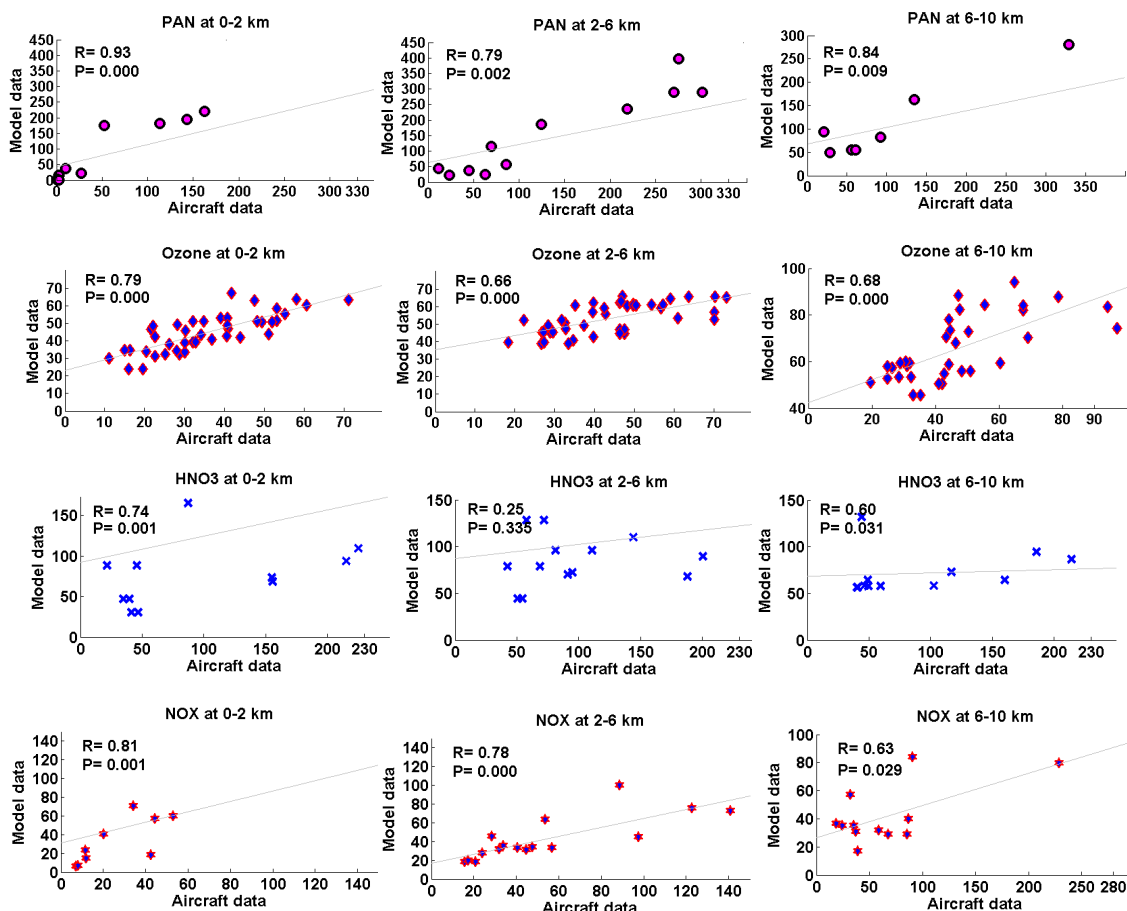


**Figure 2.** Scatter plot between model simulation (averaged for 1995–2004) and aircraft observations of PAN (ppt), ozone (ppb), HNO<sub>3</sub> (ppt) and NO<sub>x</sub> (ppt) (averaged for the monsoon season (June–September)). The model simulations and aircraft observations are averaged for altitude ranges over the coherent regions. The Pearson's correlation coefficient ( $R$ ) and corresponding  $p$ -value is given in each subplot.

### 3.2 Comparison with MIPAS-E retrievals

In order to study the influence of monsoon circulation on the distribution of PAN in the UTLS region, multi-year averages (2005–2011) of seasonal mean (June–September) PAN retrievals from MIPAS-E are analyzed. Figure 3a presents these data for the altitude range 14–16 km, and Fig. 3b shows the corresponding ECHAM5–HAMMOZ results for comparison. MIPAS-E observations show maximum PAN mixing ratios ( $\sim 200$ – $230$  ppt) over (1) the Asian monsoon anticyclone region ( $12$ – $40^\circ$  N,  $20$ – $120^\circ$  E), and (2) over parts of North America, the Gulf Stream, (3) southern Atlantic Ocean and the west coast of tropical Africa. ECHAM5–HAMMOZ CTRL simulations also show high PAN concentration at these locations; however, PAN concentrations are lower than MIPAS-E observations and appear somewhat more localized. MIPAS-E exhibits a PAN maximum originating from African sources over the South Atlantic, whereas the model shows this maximum over the African continent. This may be the outflow of biomass burning over central and southern Africa

during summer monsoon, which might be underestimated in the model. The biomass burning region of Africa during the ASM season is  $\sim 30^\circ$  S– $20^\circ$  N;  $20^\circ$  W– $30^\circ$  E (Galanter et al., 2000). The longitude–altitude and latitude–altitude cross sections of MIPAS-E observed and simulated PAN over the biomass burning region are plotted in Fig. S3. The model simulation shows that the biomass plume rising from Africa moves westward and northward over the Atlantic Ocean and merges with South American plume. From satellites, aircraft observations and model simulations, Real et al. (2010) and Barret et al. (2008) reported a plume in the middle and upper troposphere (UT) over the southern Atlantic which originates from central African biomass burning fires.

The difference between ECHAM5–HAMMOZ simulation and MIPAS-E observations are shown in Fig. S3c and f. These figures show that the model underestimates biomass burning PAN by 20–60 ppt. These differences may also be related to issues in the vertical transport of PAN, or to a possible underestimation of the emission sources of NMVOCs. Uncertainties in the rate coefficients and absorption cross

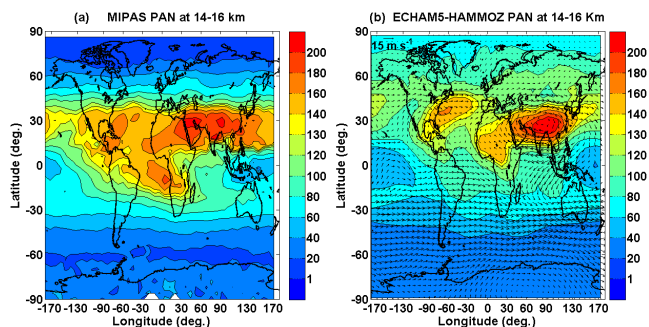


**Figure 3.** Distribution of seasonal mean PAN concentration (ppt) averaged for 14–16 km (a) observed by MIPAS-E (climatology for the period 2002–2011) (b) ECHAM5–HAMMOZ CTRL simulations. Wind vectors at 16 km are indicated by black arrows in (b).

sections of PAN may also play a role. Furthermore, anthropogenic  $\text{NO}_x$  emissions are mostly underestimated in the emission inventories (Miyazaki et al., 2012). As discussed in Fadnavis et al. (2014), UTLS PAN over the ASM is sensitive to  $\text{NO}_x$  emission changes in India or China. In their study, also performed with ECHAM5–HAMMOZ, a 73 %  $\text{NO}_x$  emission change in India lead to a PAN increase of 10–18 %, while a 73 %  $\text{NO}_x$  emission change in China changed PAN over the ASM by 18–30 %. The cross-section plots of (see Fig. S4) differences in MIPAS-E PAN with model-simulated PAN indicate that in the UTLS, MIPAS-E PAN is higher than model-simulated PAN by  $\sim 20$ –60 ppt (except at 20 km). PAN is lower by 20–40 ppt over the eastern part of ASM anticyclone (southern India and Southeast Asia) and also over Indonesia and northern Australia. In general, in the ASM region, during the monsoon season, MIPAS-E PAN is higher than the model by 30–60 ppt between 8 and 16 km and the difference between MIPAS-E and model PAN varies between +40 ppt and –40 ppt between 17 and 20 km.

## 4 Transport of PAN during monsoon season

### 4.1 Transport from the northern tropical land mass

Figure 3a shows high concentrations of MIPAS-E PAN at 14–16 km over Asia, North America and tropical Africa. ECHAM5–HAMMOZ simulations (Fig. 3b) also show similar distribution. This may be due to transport from the boundary layer into the UTLS by the monsoon convection from respective regions. ECHAM5–HAMMOZ-simulated outgoing long-wave radiation (OLR) and 850 hPa winds averaged for the monsoon season are shown in Fig. S5a. They indicate the extent of deep convection near the surface. NCEP reanalysis OLR and 850 hPa winds averaged for the monsoon season (2000–2010) are plotted in Fig. S5b for comparison. These figures indicate that the model can reproduce deep convection as well as the large-scale circulation. The cross section of distribution of simulated cloud droplet

number concentration (CDNC) and ice crystal number concentration (ICNC) over Asia, North America and tropical Africa confirms strong convective transport from these regions (Fig. S5c–e). It should be noted that vertical velocities in a large-scale model also indicate rapid uplift in deep convective regions. From satellite observations and model simulations Park et al. (2009) reported transport of fraction of boundary-layer carbon monoxide (CO) into the UTLS by the Asian monsoon convection.

To illustrate vertical transport, longitude–altitude cross sections of PAN mixing ratios averaged over the region 0–30° N for June–September as obtained from MIPAS-E and ECHAM5–HAMMOZ are shown in Fig. 4a and b, respectively. Both MIPAS-E observations and ECHAM5–HAMMOZ simulations show elevated levels of PAN (200–250 ppt) near 80–100° E (ASM), 30° W–30° E (WAM) and 80–100° W (NAM) region. The simulated PAN distribution along with winds plotted in Fig. 4b show cross-tropopause transport from these regions. It reveals that transport of boundary-layer PAN to the UTLS mainly occurs from strong convective regions, i.e., Bay of Bengal ( $\sim 80$ –90° E), South China Sea ( $\sim 100$ –120° E), western Atlantic Ocean (Gulf Stream region) and Gulf of Mexico (80–100° W). MIPAS-E observations and model simulations show that the transport due to ASM is strongest and reaches deepest into the lower stratosphere. This is due to the more intense deep convection activity over the ASM region compared to the NAM region (see Fig. S5c–e). Figure 4c presents the differences between MIPAS-E and model-simulated PAN. It appears that the model PAN is overestimated over the ASM (20–30 ppt) and underestimated over the NAM (50–70 ppt) and WAM (20–50 ppt) regions between 8 and 18 km. However, the overestimation in the UT in the ASM is difficult to explain on physical grounds and is more likely to be a MIPAS-E sampling issue as discussed later.

### 4.2 Transport from the southern tropical land mass

In order to understand transport of PAN due to southern WAM, SAM and AUSM, we show longitude–pressure sections of MIPAS-E observations and model-simulated PAN concentrations averaged over 0–25° S in Fig. 4d, e, respectively. The model has plumes near 20, 100° E and 80° W. These three regions of convective transport are (1) tropical southern Africa 10–40° E, referred to as southern Africa, (2) Indonesia and northern parts of Australia  $\sim 100$ –110° E and (3) South America  $\sim 70$ –80° W. Outflow from Indonesia and from northern parts of Australia ( $\sim 100$ ° E) penetrates deep into the UTLS. Tropical Rainfall Measuring Mission (TRMM) satellite observations show high frequency of intense overshooting convection over these areas (during the monsoon season) with highest density in the belt 0–10° S over the Caribbean, Amazon, Congo and southern maritime continent (Liu and Zipser, 2005). The analyses of vertical winds show strong transport from 10–40° E, 100–110° E,



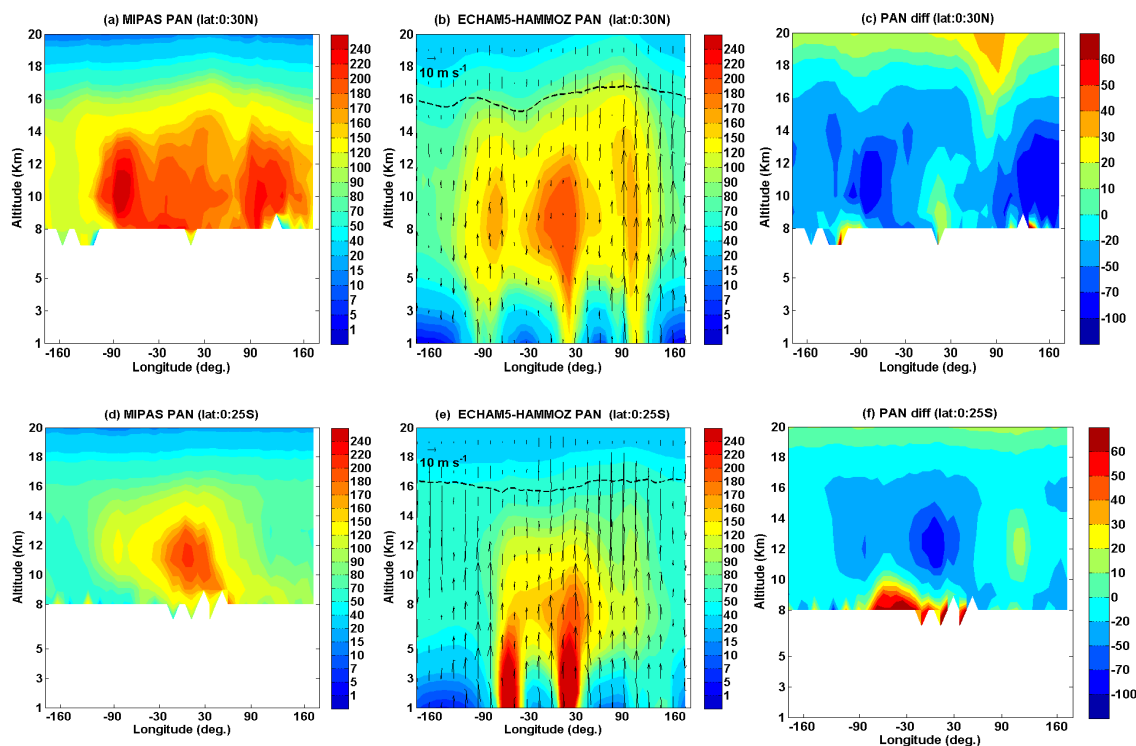


**Figure 4.** Longitude–altitude cross section of PAN (ppt) averaged for the monsoon season and  $0\text{--}30^\circ\text{N}$ ; (a) MIPAS-E climatology (b) ECHAM5–HAMMOZ CTRL simulations. (c) Difference in PAN (ppt) (MIPAS-E–ECHAM5–HAMMOZ). PAN (ppt) averaged for the monsoon season and  $0\text{--}25^\circ\text{S}$  (d) MIPAS-E climatology (e) ECHAM5–HAMMOZ CTRL simulations (f) difference in PAN (ppt) (MIPAS-E–ECHAM5–HAMMOZ). ECHAM5–HAMMOZ simulations are smoothed with averaging kernel of MIPAS-E. Wind vectors are indicated by black arrows in (b) and (e). The vertical velocity field has been scaled by 300. The black line in (b) and (e) indicates the tropopause.

$70\text{--}80^\circ\text{W}$  (in the belt  $0\text{--}10^\circ\text{S}$ ) (figure not shown). The amount of high-level cloud fraction is also high over these regions. Distribution of CDNC and ICNC show deep convection over these regions (figure not shown). The model simulations show high PAN concentrations reaching the UTLS. Thus transport due to deep convection is reasonably well captured by the model. However, the MIPAS-E retrievals only show a plume rising over southern Africa and no enhancement over the AUSM (Indonesia–Australia) and SAM regions. Figure 4e shows that the plumes from the three outflow regions are mixed in the UT (8–14 km) by the prevailing westerly winds. The reasons for a single plume seen in MIPAS-E may be that lower concentrations of PAN reach these altitudes (above 8 km) from SAM and AUSM and mix with the plume over southern Africa. There are indications of elevated PAN concentrations at the lower boundary in Fig. 4d. Simulations show lower PAN mixing ratios over the longitudes of SAM and AUSM (see Fig. 4e). The differences between MIPAS-E observations and simulations (Fig. 4f) show that model PAN is overestimated in the AUSM (10–30 ppt) and is underestimated over the southern WAM (20–70 ppt) and SAM (20–50 ppt) between 10 and 18 km. It is likely that the three-plume structure in the UT seen in the model is being obscured in the observations due to sampling

issues since periods of deep convection that reach significantly above 8 km are associated with significant cloud cover.

Figure 4 shows that simulated transport of PAN due to ASM, NAM and WAM convection is stronger and penetrates deeper into the UT compared to SAM and AUSM. This is consistent with the distribution of deep convection noted by Gettelman et al. (2002). In general, the PAN amounts in the UTLS in the model are less than those observed by MIPAS-E. This may be due to an underestimation of the chemical PAN source from VOC precursors or too little vertical transport in the model or a combination of both. Earlier model studies with ECHAM also exhibited concentrations of CO in the upper tropospheric outflow that were too low (M. Schultz, unpublished data from the NASA Global Tropospheric Experiment TRACE-P mission).

### 4.3 Transport from the Asian summer monsoon region

The ASM anticyclone extends from  $60$  to  $120^\circ\text{E}$  and  $10$  to  $40^\circ\text{N}$  (see Fig. 3b). Latitude–altitude cross sections over the ASM anticyclone ( $60\text{--}120^\circ\text{E}$ ) of MIPAS-E observed PAN (plotted in the altitude range 8–20 km) and ECHAM5–HAMMOZ CTRL simulations are shown in Fig. 5a and b, respectively. ECHAM5–HAMMOZ simulations are similar to

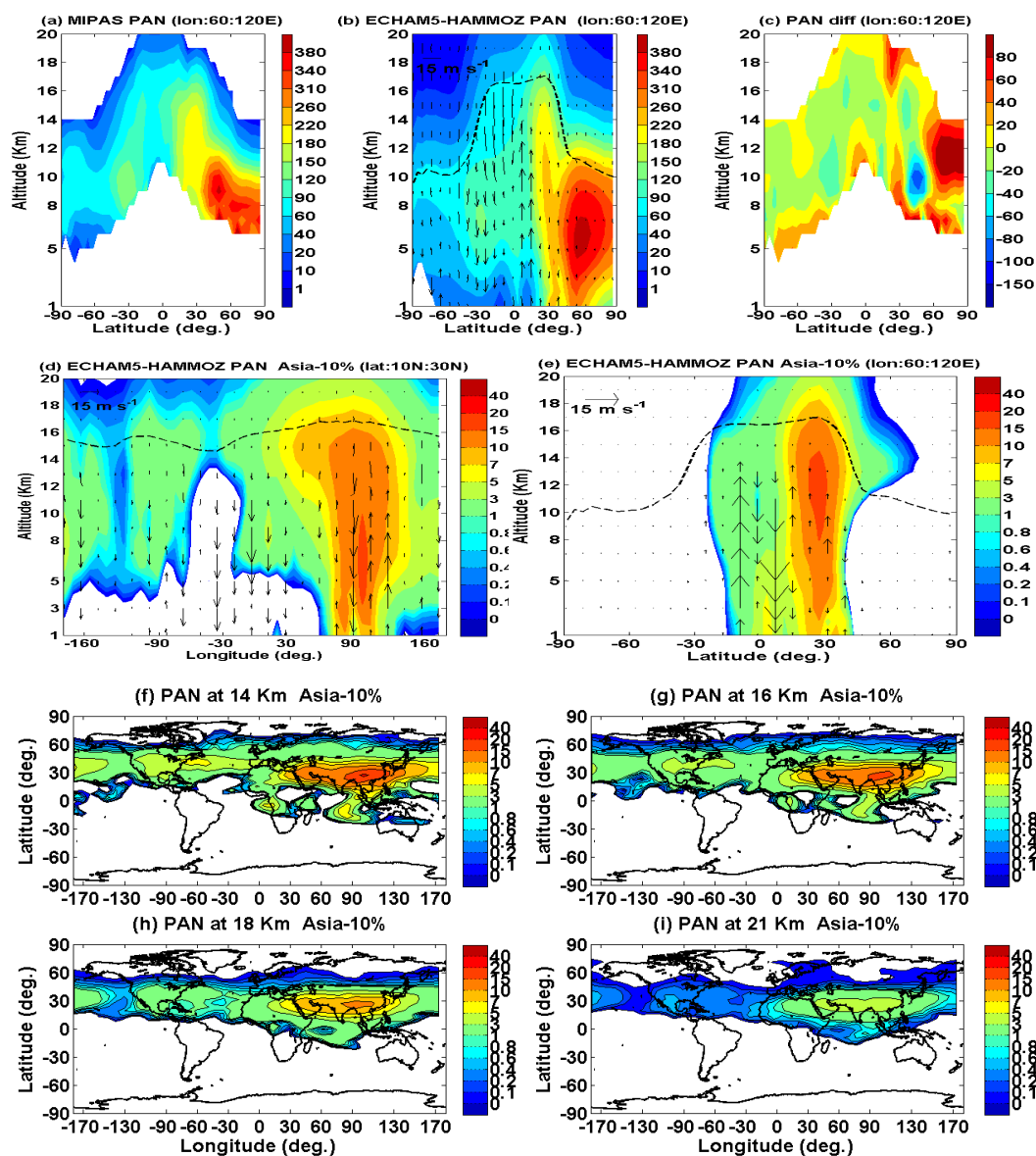


**Figure 5.** Latitude–altitude cross section of PAN (ppt) (a) MIPAS-E climatology, averaged for the monsoon season and for 60–120° E, (b) PAN from ECHAM5–HAMMOZ CTRL simulations, averaged for the monsoon season and 60–120° E, (c) difference in PAN (ppt) (MIPAS–ECHAM5–HAMMOZ), (d) longitude–altitude section averaged over 10–30° N obtained from reference–Asia –10 % simulations (e) same as (d) but latitude–altitude section averaged over 60–120° E, (f)–(i) latitude–longitude sections of reference–Asia –10 % simulations at 14, 16, 18 and 21 km, respectively. Wind vectors are indicated by black arrows. The vertical velocity field has been scaled by 300.

MIPAS-E retrievals of PAN. There is indication of plume ascent into the lower stratosphere. The ECHAM5–HAMMOZ simulations also show transport of subtropical boundary-layer PAN into the UTLS due to deep convection. This is not visible in the MIPAS-E data because of the lack of data below 8 km. Figure 5b shows that there is transport from 40–50° N reaching up to 10 km (~200 hPa). Park et al. (2004, 2007, 2009) and Randel and Park (2006) noted that trace species are introduced into the monsoon anticyclone at its eastern end around 200 hPa. The uplift over Southeast Asia

and the base of the Himalayas in India pumps tracers into the upper tropical troposphere where they get horizontally redistributed by the anticyclonic circulation and form the region of high PAN values between 40° N and high latitudes. Figure 10c shows that the mid-latitude maximum seen in Fig. 5c is due to pollution transport from Europe. The Chinese emissions are feeding into this large plume over Russia and are transported partly and diluted over the extratropical Pacific Ocean. The latitude–altitude section of differences between MIPAS-E and simulated PAN indicates that ASM plume is

underestimated in the model (see Fig. 5c). It is interesting to compare Fig. 4c (longitude–altitude section) and Fig. 5c (latitude–altitude section). The reason for underestimation of the ASM plume in the latitude–altitude section may be due to a lower contribution from the eastern part of anticyclone in the model. Figure S4 shows model PAN is underestimated over southern India and Southeast Asia in the UT, and overestimated in the lower stratosphere.

In order to understand the impact of transport from ASM region on the rest of the world, we analyze differences between reference and Asia–10% simulations (reference–Asia–10%). The latitude–altitude and longitude–altitude cross sections over the ASM region (Fig. 5d and e) show transport of  $\sim 5$ –20 ppt of PAN into the lower stratosphere. The horizontal cross sections at 14 to 21 km (Fig. 5f–i) show that Asian PAN is transported to northern Atlantic by subtropical westerly winds. These figures show that a 10% change in Asian emissions ( $\text{NO}_x$  and NMVOCs) transports  $\sim 5$ –30 ppt into the UTLS over Asia and 1–7 ppt of PAN in the UTLS of northern subtropics and mid-latitudes.

#### 4.4 Transport from the North American monsoon region

Figure 6a and b exhibit latitude–altitude sections of PAN from MIPAS-E retrievals and ECHAM5–HAMMOZ simulations (seasonal mean for July–September) over the North American monsoon region between 70 and 120° W. MIPAS-E observations and the model indicate transport of PAN into the UTLS. The distribution of ECHAM5–HAMMOZ-simulated PAN from the boundary layer to UTLS shows the source region is at around 40° N. There is convective uplift of PAN over the northern Gulf of Mexico region and over the Gulf Stream. High amount of pollutants emitted from northeast America from a number of power plants are located in Atlanta, Washington, Chicago, Boston and Jacksonville (CEC report, 2011). The tropospheric  $\text{NO}_2$  columns retrieved from the SCIAMACHY and OMI satellite instruments show high amounts of anthropogenic  $\text{NO}_2$  emissions over this region (Lamsal et al., 2011; Miyazaki et al., 2012). The model simulations show a high amount of PAN concentrations over this region (see Fig. 10a–d). The monsoon convection lifts these pollutants to the UT. The outflow of these pollutants is over the Atlantic (see Fig. 3a). TRMM precipitation radar observations show significant overshooting convective activity over this region during the monsoon season (Liu and Zipser, 2005). The vertical distribution of differences in MIPAS-E and simulated PAN shows that PAN is underestimated in the model (see Fig. 6c) over North and South America (10–60 ppt) between 10 and 18 km, however PAN is overestimated in the model between 8 and 10 km in the region near 30° N. As discussed above this may be associated with European emissions and transport.

Figure 6d–e show impact of North American emission (reference–North America–10%) on the transport of PAN.

The figure shows cross-tropopause transport of PAN by North American monsoon convection. The amount of PAN transported ( $\sim 1$ –5 ppt) into the lower stratosphere is less than for the ASM ( $\sim 10$ –20 ppt). The latitude–longitude distribution of PAN (Fig. 6f–i) shows that the upper tropospheric westerly winds transport  $\sim 1$ –10 ppt of PAN to the Atlantic, Europe and North China.

#### 4.5 Transport from the West African region

Figure 7a–b show vertical distributions of PAN over the African region (averaged over 0–45° E). MIPAS-E observations and model simulations indicate a plume that crosses the tropopause and enters the lower stratosphere. The model surface fields (see Fig. 7b) show that this plume arises from latitudes 5–20° S over Africa and that it moves equatorward. It subsequently merges with the ASM plume. A prominent tongue of high PAN values between 30 and 60° N is captured in model simulations. This feature appears to be related to emissions from Europe being transported towards the equator in the upper subtropical troposphere. However, in the model, emissions from Europe are transported poleward instead of equatorward (Fig. 7b). There is a region of strong descent in the model between 30 and 40° N (see Fig. 7b) which deforms the PAN isopleths around 12 km around 30° N. This feature is not seen in the MIPAS-E retrievals and indicates a disagreement of the model with the transport pattern of the atmosphere in this region. The transport of PAN in the 10–20° S latitude band over the Congo, Angola and Tanzania regions of southern and tropical Africa is not pronounced in the model compared to MIPAS-E observations. This behavior indicates that deep tropical convection is underestimated in the model in this latitude band. The vertical distribution of differences in MIPAS-E and simulated PAN (Fig. 7c) shows that simulated PAN is underestimated over these regions (5–20° S and 20–40° N) between 10 and 18 km. The reason may be related to underestimation of deep tropical convection in the model in this latitude band. Simulated PAN is overestimated between 8 and 12 km near the equator.

The reference–Africa–10% simulation (Fig. 7d–e) shows that African PAN is transported up to the tropopause. The cross sections over North and southern Africa show penetration of the North African plume into the lower stratosphere ( $\sim 19$  km). However, PAN transport into the lower stratosphere ( $\sim 0.2$ –0.6 ppt) is comparatively less than Asia or North America. Figure 7g–j show transport of  $\sim 5$ –50 ppt of PAN in the UT (6–12 km) of tropical Africa. There is transport from equatorial Africa to the Atlantic and Mexico between 6 and 8 km (Fig. 7g–h) which is then transported to North China by upper tropospheric (12 km) westerly winds (see Fig. 7j).

The model-simulated latitude–altitude and longitude–altitude cross sections of  $\text{NO}_x$  and  $\text{HNO}_3$  over the ASM (10–40° N, 60–120° E), NAM (10–40° N, 70–120° W) and WAM (0–25° S, 0–45° E) are shown in Fig. 8a–j, respectively. Fig-

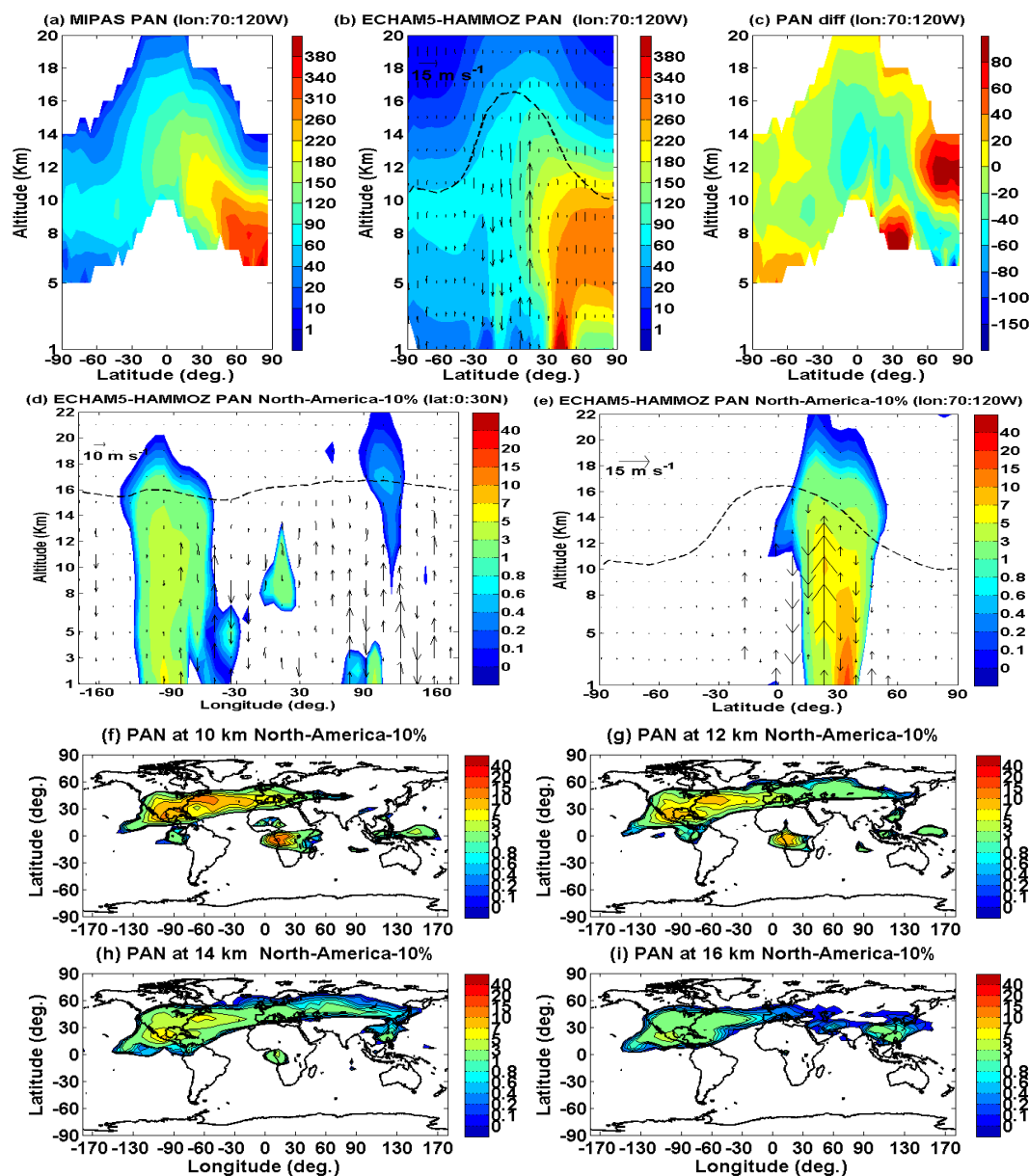


**Figure 6.** Latitude–altitude cross section of PAN (ppt) (a) MIPAS-E climatology, averaged for the monsoon season and for 70–120° W, (b) PAN from ECHAM5–HAMMOZ CTRL simulations, averaged for the monsoon season and 70–120° W, (c) difference in PAN (ppt) (MIPAS–ECHAM5–HAMMOZ), (d) longitude–altitude section averaged over 0–30° N obtained from reference–North America –10% simulations (e) same as (d) but latitude–altitude section averaged over 70–120° W, (f)–(i) latitude–longitude sections of reference–North America –10% simulations at 10, 12, 14, and 16 km, respectively. Wind vectors are indicated by black arrows. The vertical velocity field has been scaled by 300.

ure 8a–e show transport features of  $\text{NO}_x$ . These are similar to those seen in the distribution of PAN, but with sharper signatures due to the shorter lifetime of  $\text{NO}_x$ . This shows that monsoon convection lifts boundary-layer pollutants including NOy species to the UTLS. The distribution of  $\text{HNO}_3$  (see Fig. 8f–j) shows a complex pattern. Comparing Fig. 4b, the region around 100° E with intense convective uplift corresponds to  $\text{HNO}_3$  depletion from the surface to above 10 km.

In fact, the upper tropospheric region of the ASM anticyclone exhibits much lower values of  $\text{HNO}_3$  compared to all the other longitudes in the 10–40° N band (Fig. 8h). This suggests that in the model, the convective transport in the ASM region is associated with efficient removal by wet scavenging. In contrast, the North American monsoon region has  $\text{HNO}_3$  ascending to the UT with significantly less loss. This is likely due to the fact that convection involved in vertical

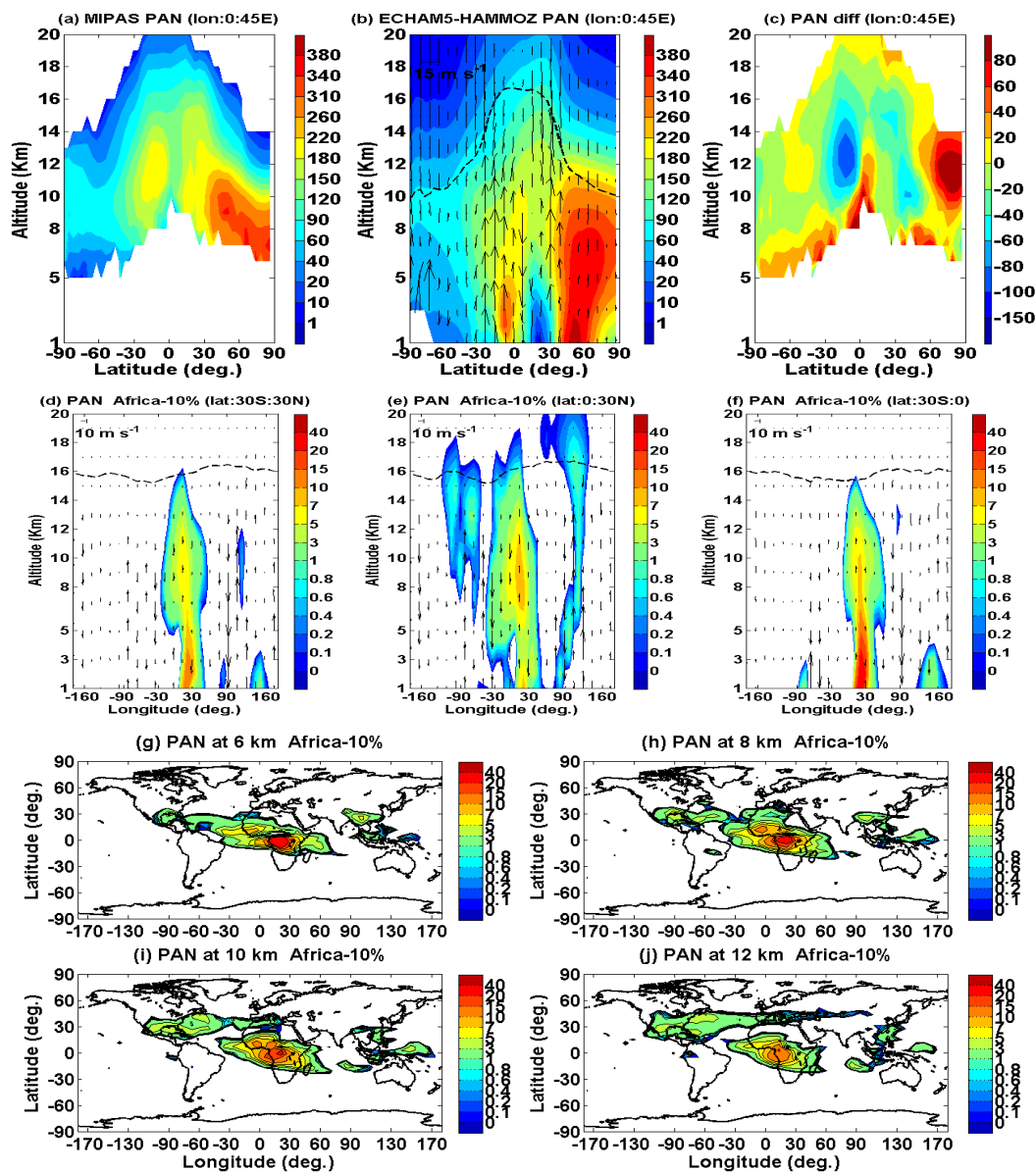
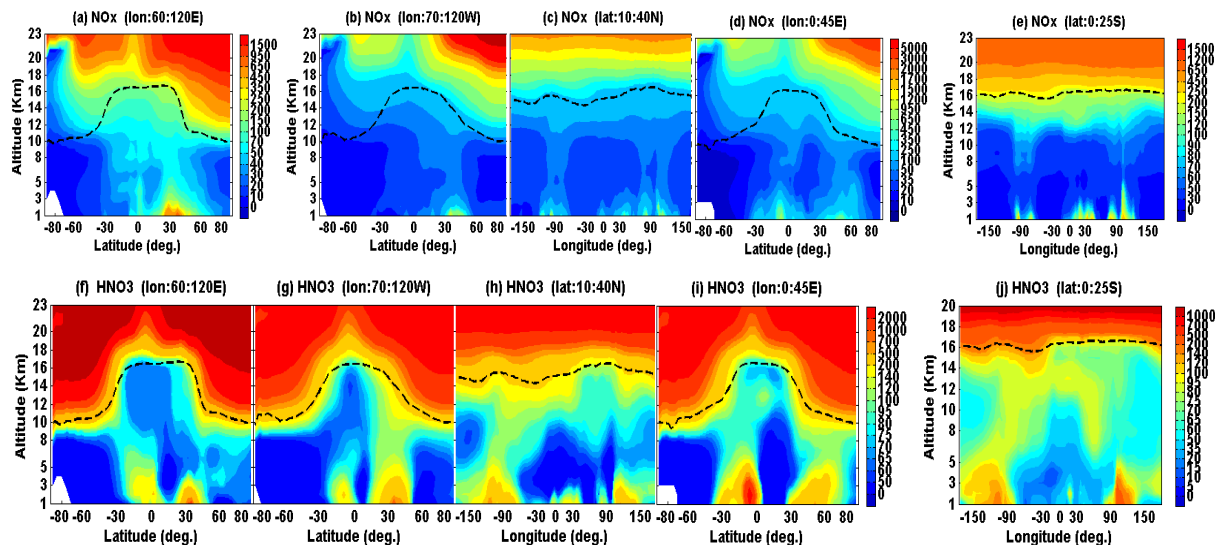


**Figure 7.** Latitude–altitude cross section of PAN (ppt) (a) MIPAS-E climatology, averaged for the monsoon season and for 0–45° E, (b) PAN from ECHAM5–HAMMOZ CTRL simulations, averaged for the monsoon season and 0–45° E, (c) difference in PAN (ppt) (MIPAS–ECHAM5–HAMMOZ), (d) longitude–altitude section averaged over 30° S–30° N obtained from reference–Africa–10% simulations (e) same as (d) but averaged over 0–30° N, (f) same as (d) but averaged over 0–30° S. Wind vectors are indicated by black arrows. The vertical velocity field has been scaled by 300. Longitude–latitude section of PAN obtained from reference–Africa–10% simulations at (g) 6 km, (h) 8 km, (i) 10 km and (j) 12 km.

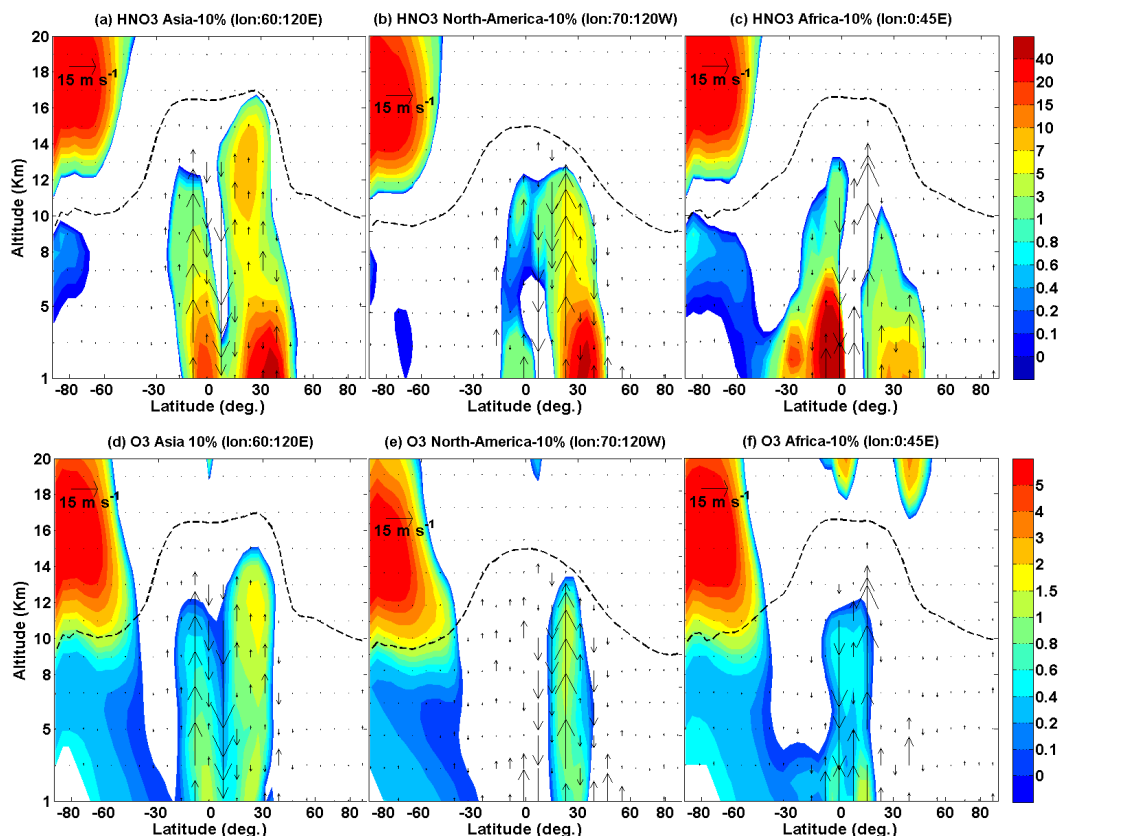
transport during the NAM is not as intense and not as deep as in the case of the ASM and there are differences in wet scavenging. Figure 8g shows that the plume rising from South America moves towards the equator but does not have the extension into the UT as the North American plume. These are June–September averages, and the intertropical convergence zone is on the Northern Hemisphere side during this period. Thus, weaker convective transport is to be expected on the Southern Hemisphere side of the equator during this period.

Figure 8i shows significant transport of African emissions around ~0–15° S and a plume rising from Europe (~35–60° N) as well.

Figure 9a–f show vertical distribution of HNO<sub>3</sub> and O<sub>3</sub> over Asia, North America and Africa as obtained from differences between the reference and Asia–10%, reference and North America–10% as well as reference and Africa–10% simulation. It is evident that transport of HNO<sub>3</sub> for Asia–10% simulation is deeper in the UT (~16 km)



**Figure 8.** (a) Latitude–altitude cross section of seasonal mean ECHAM5–HAMMOZ  $\text{NO}_x$  (ppt) averaged for (a) 60–120° E and (b) 70–120° W; (c) longitude–altitude cross section averaged over 10–40° N, (d) latitude–altitude cross section averaged over 0–45° E and (e) longitude–altitude cross section averaged over 0–25° S, (f)–(i) same as (a)–(e) but for  $\text{HNO}_3$ .



**Figure 9.** Latitude–altitude variation of (a)  $\text{HNO}_3$  (reference–Asia –10 %), averaged over 60–120° E (b)  $\text{HNO}_3$  (difference of reference–North America –10 %), averaged over 70–120° W (c)  $\text{HNO}_3$  (reference–Africa –10 %), averaged over 0–45° E (d)  $\text{O}_3$  (difference of reference–Asia –10 %) averaged over 60–120° E (e)  $\text{O}_3$  (reference–North America –10 %) over North America averaged over 70–120° W (f)  $\text{O}_3$  (reference–Africa –10 %) over Africa averaged over 0–45° E (reference–Africa –10 %).  $\text{HNO}_3$  is expressed in ppt and ozone in ppb.

than North America –10 % and Africa –10 % simulations. It can be seen that Asia –10 %, North America –10 % and Africa –10 % simulations transport  $\sim 7$ – $10$  ppt,  $\sim 5$ – $7$  ppt and  $\sim 3$ – $5$  ppt of  $\text{HNO}_3$  in the UT of their respective regions.

In the UT, between 6 and 10 km, Asia –10 % simulation shows transport of  $\sim 10$ – $15$  ppt of  $\text{HNO}_3$  over the western Pacific and  $\sim 3$ – $10$  ppt over tropical America by the subtropical westerly winds (figure not included). North America –10 % simulation shows transport of  $\sim 5$ – $7$  ppt of  $\text{HNO}_3$  over the Atlantic, North Africa, Saudi Arabia and North China by the subtropical westerly winds and  $\sim 3$ – $5$  ppt of  $\text{HNO}_3$  over the equatorial Pacific, Indonesia, China and India by the tropical easterly winds. Africa –10 % simulation shows transport of  $\sim 3$ – $5$  ppt  $\text{HNO}_3$  from North Africa to North America and the equatorial Pacific; there is also transport of  $\sim 4$  ppt of  $\text{HNO}_3$  from southern Africa to the Atlantic, South America, Indonesia, China and India by the tropical easterly winds (figure not included).

North America –10 % simulation shows transport of boundary-layer ozone extending up to the tropopause, which is higher than for the Asia –10 % and Africa –10 % simulations (Fig. 9d–f). Asia –10 %, North America –10 % and Africa –10 % simulations show transport  $\sim 1$ – $2$ ,  $\sim 0.8$ – $1.5$  and  $\sim 0.4$ – $0.6$  ppb of ozone in the UT of their respective regions.

In the UT, between 6 and 10 km, Asia –10 % simulation shows transport of ozone  $\sim 1.5$  ppb to the western Pacific and 0.8 ppb to Mexico and United States by the subtropical westerly winds (figure not included). North America –10 % simulation shows transport of 0.4–1.5 ppb of  $\text{O}_3$  to the equatorial Pacific extending up to Indonesia by the tropical easterly winds. There is some outflow ( $\sim 0.6$  ppb) over the Atlantic by the subtropical westerly winds as well (figure not included). Africa –10 % simulation shows transport of  $\sim 0.4$ – $0.8$  ppb of ozone to equatorial Atlantic and Mexico (figure not included).

It can be seen that similar emission change over Asia, North America and Africa causes highest change in  $\text{HNO}_3$  and ozone in the UT over Asia and least over Africa. In the UT, between 6 and 10 km, transport of  $\text{HNO}_3$  by Asia –10 % ( $\sim 3$ – $10$  ppt of  $\text{HNO}_3$  to tropical America) is higher than North America –10 % ( $\sim 3$ – $7$  ppt of  $\text{HNO}_3$  to China and India) and Africa –10 % ( $\sim 3$ – $5$  ppt of  $\text{HNO}_3$  to tropical America, China and India). Similarly ozone transport is higher for Asia –10 % than North America –10 % and Africa –10 % simulations.

#### 4.6 Horizontal transport

PAN concentrations from MIPAS-E and ECHAM5–HAMMOZ at different altitudes are analyzed to investigate horizontal transport. Figure 10a shows the distribution of PAN from ECHAM5–HAMMOZ simulations near the surface (2 km). Sources of PAN are apparent over South America, southern Africa, North America, Europe, Russia

and northern China/Mongolia. The PAN distribution at 4 km (see Fig. 10b) shows high concentrations above these regions indicating vertical transport. Figure 10c and d show the distribution at 6 and 8 km. The upper level anticyclonic circulation between  $10^\circ\text{N}$  and  $30^\circ\text{S}$  over the Atlantic transports PAN from central Africa towards America and from Brazil towards southern Africa. The large-scale Biosphere–Atmosphere Regional Experiment in Amazonia (LBA-CLAIRE-98) campaign observations (Andreae et al., 2001) and African Monsoon Multidisciplinary Analysis (AMMA) project (Real et al., 2010) show that the biomass burning plume originating from Brazil is lifted to altitudes around 10 km. This plume is entrained into deep convection over the northern Amazon, transported out over the Atlantic and then returned to South America by the circulation around a large upper-level anticyclone. This transport is well captured by the model.

North American pollution also gets transported by the westerly winds over Eurasia, forming an organized belt. This transport pattern persists up to 12 km (Fig. 10e and g). MIPAS-E observations at 12 km also show this transport pattern. The source region for the PAN from southern Africa is the region of active biomass burning. Since this region is located in the tropics, the outflow is over the Atlantic due to the prevailing easterly winds. ECHAM5–HAMMOZ simulations show similar transport (see Fig. 10e). But there are differences; in particular the transport over tropical Africa does not get displaced over the Atlantic Ocean. As noted above, there are significant transport differences between the model and observations in this longitude band. Another difference is that PAN is not transported westward over Central America and towards the Pacific Ocean.

Figure 10f–h show the distribution of PAN from ECHAM5–HAMMOZ simulations and MIPAS-E retrievals, in the lower stratosphere (18 km). In both data sets PAN is transported westwards from ASM, NAM and WAM by prevailing easterly winds and maximizes in the region of the ASM anticyclone.

As can be seen from the above discussions, the ASM, NAM and WAM outflow and convection over the Gulf Stream play an important role in the transport of boundary-layer pollution into the UTLS. Previous studies (e.g., Fadnavis et al., 2013) indicated that over the Asian monsoon region, transport into the lower stratosphere occurs and there is significant vertical transport over the southern slopes of the Himalayas (Fu et al., 2006; Fadnavis et al., 2013) and also over the region spanned by the Bay of Bengal and the South China Sea (Park et al., 2009). Pollutant transport due to North American convection and tropical African outflow does not penetrate as deep into the stratosphere as the ASM; however, there is a clear indication that in the UT, middle-latitude westerly winds connect the North American pollution to the ASM.

Figures 3–7 and Fig. 10 show that in the UT, westerly winds drive North American and European pollutants east-

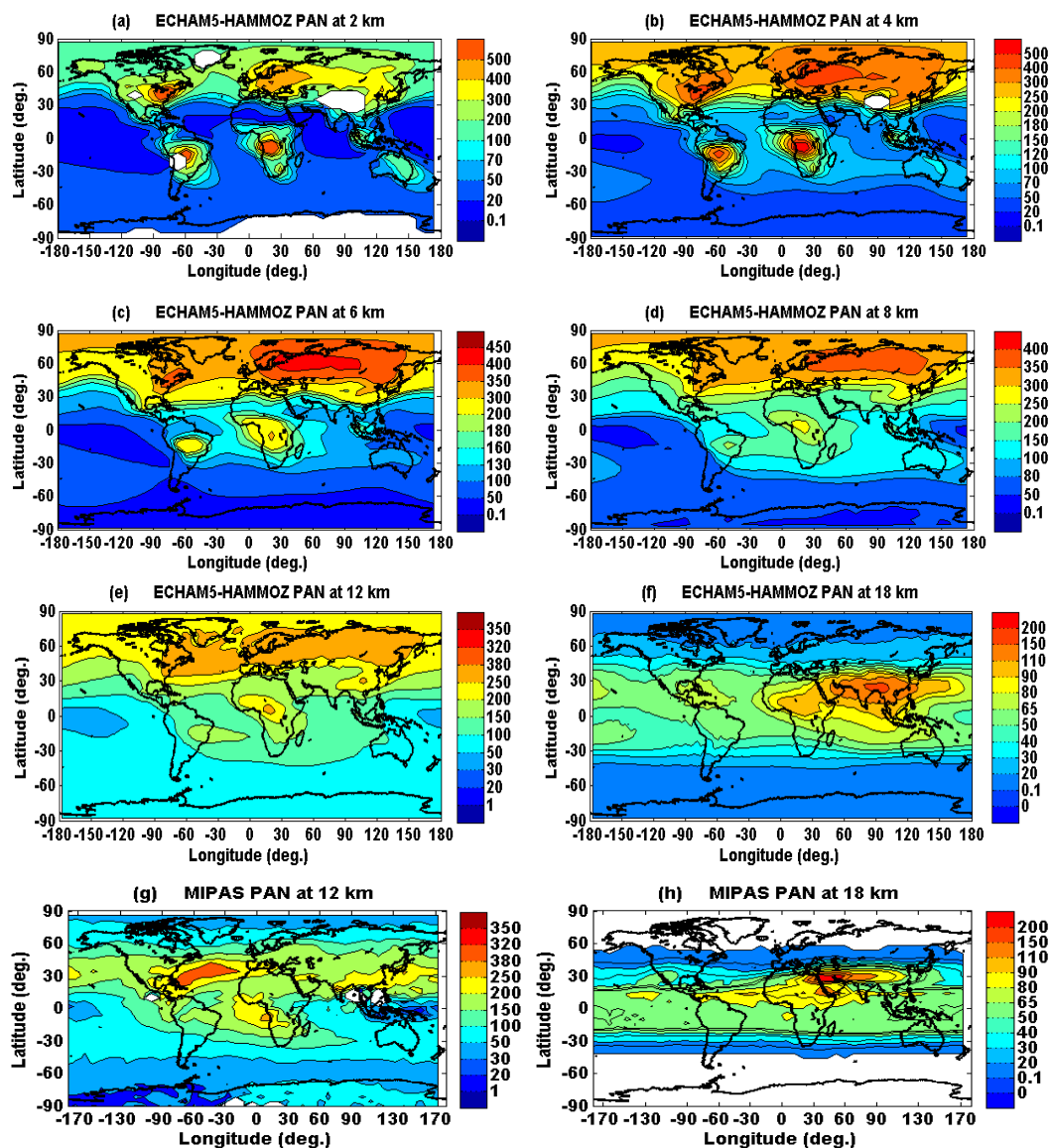


**Figure 10.** Latitude–longitude cross section of PAN (ppt) averaged for the monsoon season (a) ECHAM5–HAMMOZ simulations at 2 km (b) 4 km (c) 6 km (d) 8 km (e) 12 km and (f) 8 km. MIPAS-E climatology at (g) 12 km and (h) 18 km.

ward to at least partly merge with the ASM plume. Strong ASM convection transports these remote and regional pollutants into the stratosphere. The Caribbean is a secondary source of pollutant transport into the stratosphere. In the stratosphere the injected pollutants are transported westward by easterly winds and into the southern subtropics by the Brewer–Dobson circulation.

## 5 Impact of lightning on tropospheric PAN, $\text{NO}_x$ , $\text{HNO}_3$ and ozone

In the ASM region and during the monsoon season, the  $\text{NO}_x$  released from intense lightning activity enhances the for-

mation of PAN,  $\text{HNO}_3$  and ozone in the middle and upper troposphere which is already relatively strong due to the intense solar radiation along with high background concentrations of  $\text{NO}_x$ ,  $\text{HO}_x$  and NMVOCs (Tie et al., 2001). PAN,  $\text{HNO}_3$  and  $\text{O}_3$  produced from lightning may get transported in the lower stratosphere by deep monsoon convection and contribute to anthropogenic emission transport of these species. In order to understand contribution of lightning and the dominating lightning production regions, we analyze the difference between control and light-off simulations. Figure 11a–d show the percentage changes in model-simulated ozone,  $\text{HNO}_3$ , PAN and  $\text{NO}_x$  due to lightning as zonally averaged spatial distribution of seasonal mean (June–September) mixing ratios. The analysis indicates that



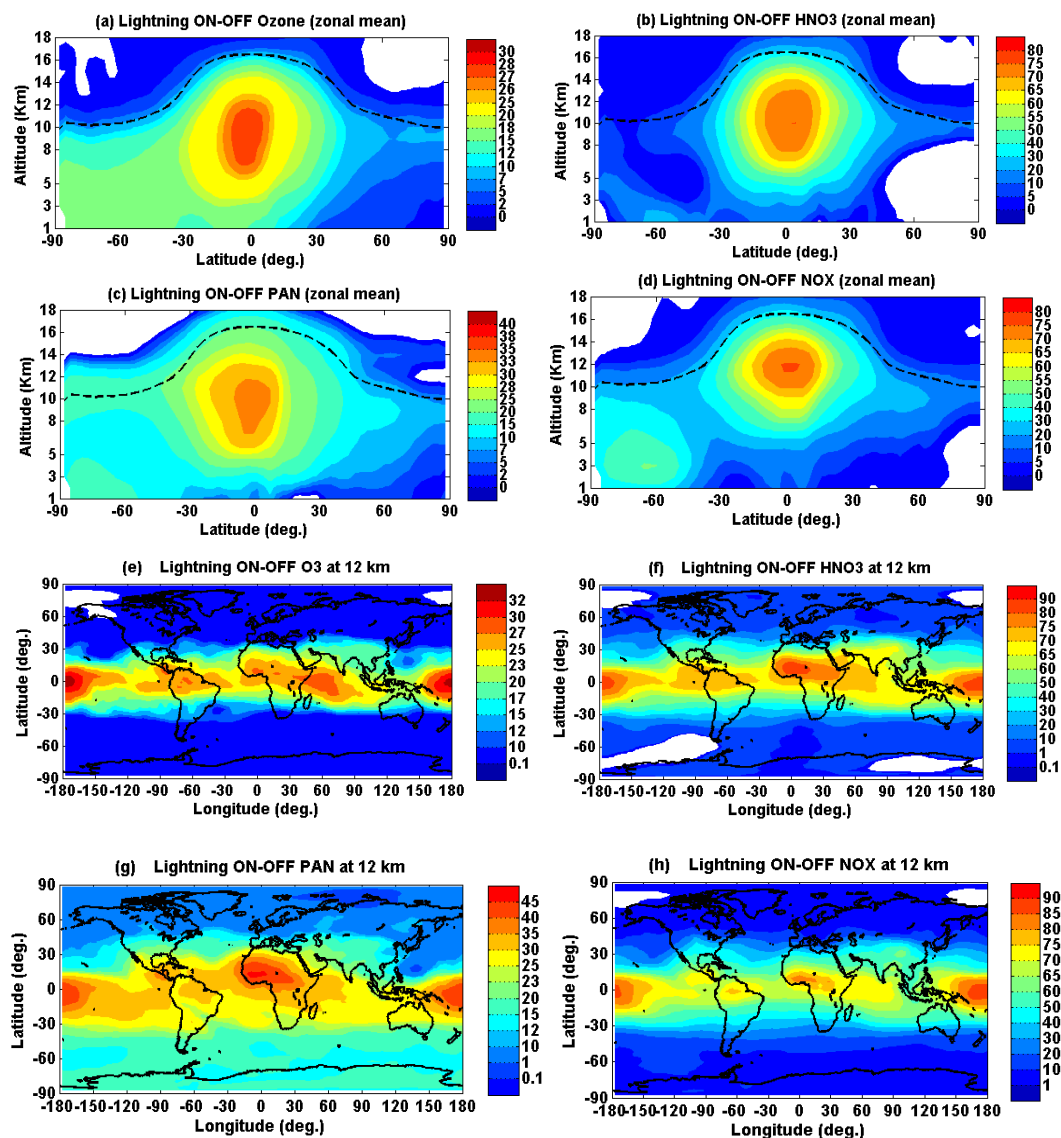


**Figure 11.** Zonal averaged seasonal mean changes (percentage) produced from lightning in (a) ozone (b) HNO<sub>3</sub> (c) PAN and (d) NO<sub>x</sub>; distribution of seasonal mean changes (percentage) produced from lightning in (e) ozone (f) HNO<sub>3</sub> (g) PAN and (h) NO<sub>x</sub> at 12 km.

the impact of lightning on these species is largest in the tropical UT between 40° N and 40° S and between 8 and 14 km. In the tropical mid-troposphere, lightning-produced maximum ozone is ~ 15–25 % (12–24 ppb), HNO<sub>3</sub> ~ 40–60 % (50–90 ppt) ~ PAN ~ 15–25 % (70–140 ppt) and NO<sub>x</sub> ~ 20–40 % (10–35 ppt), while in the UT ozone is ~ 20–30 % (20–28 ppb), HNO<sub>3</sub> ~ 60–75 % (80–110 ppt), PAN ~ 28–35 % (120–170 ppt), and NO<sub>x</sub> ~ 50–75 % (20–65 ppt). Our results are consistent with model simulations by Tie et al. (2001) and Labrador et al. (2005). The spatial distributions of NO<sub>x</sub>, ozone, PAN and HNO<sub>3</sub> produced from lightning (see Fig. 11e–h) indicate that in the UT (12 km) increases in O<sub>3</sub> ~ 20–25 % (11–17 ppbv), HNO<sub>3</sub> ~ 40–70 %, PAN ~ 25–35 % and NO<sub>x</sub> ~ 55–75 %, over North America

are in agreement with previous studies (e.g Labrador et al., 2005; Hudman et al. 2007; Zhao et al., 2009; Cooper et al., 2009); over equatorial Africa (PAN 30–45 %, HNO<sub>3</sub> ~ 70–80 %, O<sub>3</sub> ~ 25 %, NO<sub>x</sub> ~ 70 %) they agree well with Barret et al. (2010) and Bouarar et al. (2011) and over the ASM region (PAN ~ 25 %, HNO<sub>3</sub> ~ 65–70 %, O<sub>3</sub> ~ 20 %, NO<sub>x</sub> ~ 60–70 %) they agree with Tie et al. (2001). These regions coincide with regions of convective vertical transport of PAN (as seen in Figs. 4 and 5). Lightning-produced PAN will be lifted into the lower stratosphere by the monsoon convection along with anthropogenic emissions and will redistribute in the tropical lower stratosphere. Latitude–longitude cross sections of lightning-induced PAN, NO<sub>x</sub>, ozone and HNO<sub>3</sub> formation at altitudes between 8 and 14 km show that the

production of PAN,  $\text{NO}_x$ , ozone and  $\text{HNO}_3$  is less over the ASM region than over the equatorial Americas and Africa (also seen in Fig. 11). The high amounts of PAN over the ASM are therefore primarily due to anthropogenic emission transport into the UTLS from the source regions in southern and eastern Asia. As discussed in Fadnavis et al., 2014,  $\text{NO}_x$  emissions are estimated to have changed by 38 % in India and 76 % in China, respectively, during the 2002–2011 period. From sensitivity simulations they deduced that corresponding changes in upper tropospheric PAN are >40 %,  $\text{O}_3$  by >25 % and  $\text{HNO}_3$  by >70 % over the Asian monsoon region. These effects are larger than the impact of lightning  $\text{NO}_x$  emissions over this region (Fig. 11e–h).

## 6 Conclusions

In this study statistical analysis of simulated and satellite-retrieved mixing ratios of PAN,  $\text{NO}_x$ , and  $\text{HNO}_3$  is presented in order to determine the transport patterns of pollution into the Asian monsoon region and the impact of pollution flowing out of the ASM into other regions of the global atmosphere. The analysis focused on the upper troposphere and lower stratosphere and covered the period 2002–2011. In ECHAM5–HAMMOZ simulations both  $\text{NO}_x$  and NMVOCs emission were simultaneously reduced by 10 % over ASM, NAM and WAM to understand transport pathways and their relative contribution the UTLS. As discussed in Fadnavis et al. (2014),  $\text{NO}_x$  emissions are estimated to have changed by 38 % in India and 76 % in China, respectively, during this period. From sensitivity simulations they deduced corresponding changes in upper tropospheric PAN >40 %,  $\text{O}_3$  by >25 % and  $\text{HNO}_3$  by >70 % over the ASM region. These effects are larger than the impact of lightning  $\text{NO}_x$  emissions over this region, discussed in Sect. 3 of this study.

Interestingly, the ECHAM5–HAMMOZ reference simulation reveals that in the UT, westerly winds drive North American and northward-propagating southern African pollutants eastward where they mix with the ASM plume. Deep convection and strong diabatic upwelling in the ASM convectively transports a part of these plumes into the lower stratosphere. The Caribbean region is another source of pollution transport into the stratosphere. Some cross-tropopause transport occurs due to convection over North America and southern Africa as well. In the lower stratosphere, the injected pollutants from ASM, WAM and NAM are transported westward by easterly winds and into the Southern Hemisphere subtropics by the Brewer–Dobson circulation. The emission sensitivity simulations Asia–10 %, North America–10 % and Africa–10 % confirm these transport pathways. In the Southern Hemisphere, plumes rising from convective zones of southern Africa, South America and Indonesia–Australia are evident in the model simulations, but are not seen in the MIPAS-E retrievals. PAN concentrations are higher in the plume rising from southern Africa than SAM and AUSM. In

the UT, they merge by the prevailing westerly winds. MIPAS-E observations in the UTLS show a single plume over southern Africa and no enhancement over SAM or AUSM. The reasons for the single plume seen in MIPAS-E may be that although there is uplifting by each of the three monsoon systems lower concentrations of PAN reach these altitudes (above 8 km) from SAM and AUSM until they merge with the southern African plume. It is also possible that the three-plume structure in the UT seen in the model is being obscured in the observations due to sampling issues. Convective cloud cover is strongly associated with deep convection in the ASM region. The MIPAS-E data have a PAN minimum in the UT right in the longitude band of the deep convection over the southern flanks of the Himalayas (Fig. 4a). This feature is unphysical and clearly identifies a sampling bias; however, the model does not also fully reproduce the latitudinal structure of the PAN in the ASM region UTLS, which indicates that there are differences in both the distribution of convection and the large-scale circulation.

The horizontal transport of PAN analyzed from ECHAM5–HAMMOZ simulations show that the PAN from southern Africa and Brazil is transported towards America by the circulation around a large upper-level anticyclone and then lifted to the UTLS in the NAM region. This is also evident in the Africa–10 % simulation.

The vertical distribution of simulated  $\text{HNO}_3$  over the monsoon regimes shows low concentrations above 10 km at the foothills of the Himalayas. In contrast, the results show strong uplifting of  $\text{HNO}_3$  into the UT with NAM convection. This may be due to the fact that NAM convection is not as intense as the ASM and there may be more wet removal of nitrogen oxides in the ASM convection. The model simulations indicate a higher efficiency of  $\text{NO}_x$  conversion to  $\text{HNO}_3$  over the Indian region compared to NAM.

The change in emission (both  $\text{NO}_x$  and NMVOCs emissions were simultaneously reduced by 10 %) over each of the ASM, WAM and NAM regions shows that Asia–10 % transports ~5–30 ppt of PAN in the UTLS over Asia and ~1–10 ppt in the UTLS northern subtropics and mid-latitudes. North America–10 % simulation shows transport of ~1–5 ppt of PAN over the Atlantic, Europe and North China (between 12 and 14 km) and 0.4–3 ppt over Asia (nearly 16 km). Africa–10 % simulation shows transport from equatorial Africa to the Atlantic and North America between 6 and 8 km, which is then transported to Asia by upper tropospheric westerly winds (near 12 km).

Transport of  $\text{HNO}_3$  is deeper in the UT (~16 km) in Asia–10 % simulation than North America–10 % and Africa–10 % simulations. Asia–10 %, North America–10 % and Africa–10 % simulations show transport of ozone ~1–2 ppt, 0.8–1.5 ppt and 0.4–0.6 ppt in the UT over respective regions.

In the UT between 6 and 10 km, transport of  $\text{HNO}_3$  by Asia–10 % (~3–10 ppt of  $\text{HNO}_3$  to tropical America) is higher than North America–10 % (transport of 3–7 ppt of

HNO<sub>3</sub> to China and India) and Africa –10 % (~3–5 ppt of HNO<sub>3</sub> to tropical America, China and India) simulations. Similarly transport of ozone is higher for Asia –10 % than North America –10 % and Africa –10 % simulations. Comparison of emission change over Asia, North America and Africa shows highest transport of HNO<sub>3</sub> and ozone in the UT over Asia and least over Africa.

Lightning production of NO<sub>x</sub> may enhance PAN concentrations in the UT and affect its transport into the lower stratosphere. The percentage change in lightning-produced ozone, HNO<sub>3</sub>, PAN and NO<sub>x</sub> has been evaluated with a sensitivity simulation. In the UT, lightning causes significant increases in these species over equatorial America, equatorial Africa and the ASM region. These regions coincide with intense convective zones with significant vertical transport. Lightning production is higher over equatorial Africa and America compared to the ASM. However, the vertical distribution shows that higher amounts of PAN are transported into the UT in the ASM region. This indicates that the contribution of anthropogenic emissions to PAN in the UTLS over the ASM is higher than that of lightning. This is consistent with the fact that anthropogenic emissions in the ASM region are higher than in the NAM and WAM (Lamsal et al., 2011; Miyazak et al., 2012).

**The Supplement related to this article is available online at doi:10.5194/acp-15-11477-2015-supplement.**

*Acknowledgements.* The authors thank the MIPAS-E teams for providing data and the High Power Computing Centre (HPC) in IITM, Pune, India, for providing computer resources. Authors are also thankful to anonymous reviewers and the Editor for their valuable suggestions.

Edited by: F. Khosrawi

## References

- Andreae, M. O., Artaxo, P., Fischer, H., Freitas, S. R., Grégoire, J.-M., Hansel, A., Hoor, P., Kormann, R., Krejci, R., Lange, L., Lelieveld, J., Lindinger, W., Longo, K., Peters, W., de Reus, M., Scheeren, B., Silva Dias, M. A. F., Ström, J., van Velthoven, P. F. J., and Williams, J. E.: Transport of biomass burning smoke to the upper troposphere by deep convection in the equatorial region, *Geophys. Res. Lett.*, 28, 951–958, 2001.
- Arnold, F. and Hauck, G.: Lower stratosphere trace gas detection using aircraft-borne active chemical ionization mass spectrometry, *Nature*, 315, 307–309, doi:10.1038/315307a0, 1985.
- Barret, B., Ricaud, P., Mari, C., Attié, J.-L., Bousserez, N., Josse, B., Le Flochmoën, E., Livesey, N. J., Massart, S., Peuch, V.-H., Piacentini, A., Sauvage, B., Thouret, V., and Cammas, J.-P.: Transport pathways of CO in the African upper troposphere during the monsoon season: a study based upon the assimilation of spaceborne observations, *Atmos. Chem. Phys.*, 8, 3231–3246, doi:10.5194/acp-8-3231-2008, 2008.
- Barret, B., Williams, J. E., Bouarar, I., Yang, X., Josse, B., Law, K., Pham, M., Le Flochmoën, E., Lioussé, C., Peuch, V. H., Carver, G. D., Pyle, J. A., Sauvage, B., van Velthoven, P., Schlager, H., Mari, C., and Cammas, J.-P.: Impact of West African Monsoon convective transport and lightning NO<sub>x</sub> production upon the upper tropospheric composition: a multi-model study, *Atmos. Chem. Phys.*, 10, 5719–5738, doi:10.5194/acp-10-5719-2010, 2010.
- Barth, M. C., Lee, J., Hodzic, A., Pfister, G., Skamarock, W. C., Worden, J., Wong, J., and Noone, D.: Thunderstorms and upper troposphere chemistry during the early stages of the 2006 North American Monsoon, *Atmos. Chem. Phys.*, 12, 11003–11026, doi:10.5194/acp-12-11003-2012, 2012.
- Bouarar, I., Law, K. S., Pham, M., Lioussé, C., Schlager, H., Hamburger, T., Reeves, C. E., Cammas, J.-P., Nédélec, P., Szopa, S., Ravegnani, F., Viciani, S., D'Amato, F., Ulanovsky, A., and Richter, A.: Emission sources contributing to tropospheric ozone over Equatorial Africa during the summer monsoon, *Atmos. Chem. Phys.*, 11, 13395–13419, doi:10.5194/acp-11-13395-2011, 2011.
- Carmichael, G. R., Tang Y., Kurata G., Uno I., Streets D., Woo J.-H., Huang H., Yienger J., Lefer B., Shetter R., Blake D., Atlas E., Fried A., Apel E., Eisele F., Cantrell C., Avery M., Barrick J., Sachse G., Brune W., Sandholm S., Kondo Y., Singh H., Talbot R., Bandy A., Thornton D., Clarke A., and Heikes B.: Regional-scale chemical transport modeling in support of the analysis of observations obtained during the TRACE-P experiment, *J. Geophys. Res.*, 108, 8823, doi:10.1029/2002JD003117, 2003.
- CEC (Commission for Environmental Cooperation) report on North American Power Plant Air Emissions, Commission for Environmental Cooperation, 2011, 1–54, ISBN: 978-2-89700-008-0, October 2011.
- Chang, C.-P., Ding, Y., Lau, G., Ngar-Cheung, Johnson, R. H., Wang, B., and Yasunari, T.: The Global Monsoon System: Research and Forecast (2nd Edition), edited by: Chang, C.-P., Ding, Y., Lau, G., Ngar-Cheung, Johnson, R. H., Wang, B., and Yasunari, T., World Scientific Publishing Co, 2011.
- Cheng, T., Peng, Y., Feichter, J., and Tegen, I.: An improvement on the dust emission scheme in the global aerosol-climate model ECHAM5-HAM, *Atmos. Chem. Phys.*, 8, 1105–1117, doi:10.5194/acp-8-1105-2008, 2008.
- Choi, Y., Kim, J., Eldering, A., Osterman, G., Yung, Y. L., Gu, Y., and Liou, K. N.: Lightning and anthropogenic NO<sub>x</sub> sources over the United States and the western North Atlantic Ocean: impact on OLR and radiative effects, *Geophys. Res. Lett.*, 36, L17806, doi:10.1029/2009GL039381, 2009.
- Collier J. C. and Zhang G. J.: Simulation of the North American Monsoon by the NCAR CCM3 and Its Sensitivity to Convection Parameterization, *J. Climate*, 19, 2851–2866, 2006.
- Cooper, O. R., Eckhardt, S., Crawford, J. H., Brown, C. C., Cohen, R. C., Bertram, T. H., Wooldridge, P., Perring, A., Brune, W. H., Ren, X., Brunner, D., and Baughcum, S. L.: Summer-time buildup and decay of lightning NO<sub>x</sub> and aged thunderstorm outflow above North America, *J. Geophys. Res.*, 114, D01101, doi:10.1029/2008JD010293, 2009.

- Dentener, F., Kinne, S., Bond, T., Boucher, O., Cofala, J., Generoso, S., Ginoux, P., Gong, S., Hoelzemann, J. J., Ito, A., Marelli, L., Penner, J. E., Putaud, J.-P., Textor, C., Schulz, M., van der Werf, G. R., and Wilson, J.: Emissions of primary aerosol and precursor gases in the years 2000 and 1750 prescribed data-sets for AeroCom, *Atmos. Chem. Phys.*, 6, 4321–4344, doi:10.5194/acp-6-4321-2006, 2006.
- Dickerson, R. R., Huffman, G. J., Luke, W. T., Nunnermacker, L. J., Pickering, K. E., Leslie, A., Lindsey, C., Slinn, W., Kelly, T., Daum, P., Delany, A., Grennberg, J., Zimmerman, P., Boatman, J., Ray, J., and Stedman, D.: Thunderstorms: An important mechanism in the transport of air pollutants, *Science*, 235, 460–465, 1987.
- Drummond, J. W., Ehhalt, D. H., and Volz, A.: Measurements of nitric oxide between 0–12 km altitude and 67° N–60° S latitude obtained during STRAT0Z III, *J. Geophys. Res.*, 93, 15831–15849, 1988.
- Emmons, L. K., Hauglustaine, D. A., Muller, J.-F., Carroll, M. A., Brasseur, G. P., Brunner, D., Staehelin, J., Thouret, V., and Marenco, A.: Data composites of tropospheric ozone and its precursors from aircraft measurements, *J. Geophys. Res.*, 105, 20497–20538, 2000.
- Evelt, R. R., Mohrle C. R., Hall B. L., Brown T. J., and Stephens S. L.: The effect of monsoonal atmospheric moisture on lightning fire ignitions in southwestern North America, *Agr. Forest Meteorol.*, 148, 1478–1487, 2008.
- Fadnavis, S., Semeniuk, K., Pozzoli, L., Schultz, M. G., Ghude, S. D., Das, S., and Kakatkar, R.: Transport of aerosols into the UTLS and their impact on the Asian monsoon region as seen in a global model simulation, *Atmos. Chem. Phys.*, 13, 8771–8786, doi:10.5194/acp-13-8771-2013, 2013.
- Fadnavis, S., Schultz, M. G., Semeniuk, K., Mahajan, A. S., Pozzoli, L., Sonbawne, S., Ghude, S. D., Kiefer, M., and Eckert, E.: Trends in peroxyacetyl nitrate (PAN) in the upper troposphere and lower stratosphere over southern Asia during the summer monsoon season: regional impacts, *Atmos. Chem. Phys.*, 14, 12725–12743, doi:10.5194/acp-14-12725-2014, 2014.
- Fiore, A. M., Horowitz, L. W., Purves, D. W., Levy II, H., Evans, M. J., Wang, Y., Li, Q., and Yantosca, R. M.: Evaluating the contribution of changes in isoprene emissions to surface ozone trends over the eastern United States, *J. Geophys. Res.*, 110, D12303, doi:10.1029/2004JD005485, 2005.
- Fischer, E. V., Jacob, D. J., Yantosca, R. M., Sulprizio, M. P., Millet, D. B., Mao, J., Paulot, F., Singh, H. B., Roiger, A., Ries, L., Talbot, R. W., Dzepina, K., and Pandey Deolal, S.: Atmospheric peroxyacetyl nitrate (PAN): a global budget and source attribution, *Atmos. Chem. Phys.*, 14, 2679–2698, doi:10.5194/acp-14-2679-2014, 2014.
- Fischer, H. and Oelhaf, H.: Remote sensing of vertical profiles of atmospheric trace constituents with MIPAS limb-emission spectrometers, *Appl. Optics*, 35, 2787–2796, 1996.
- Fischer, H., Birk, M., Blom, C., Carli, B., Carlotti, M., von Clarmann, T., Delbouille, L., Dudhia, A., Ehhalt, D., Endemann, M., Flaud, J. M., Gessner, R., Kleinert, A., Koopman, R., Langen, J., López-Puertas, M., Mosner, P., Nett, H., Oelhaf, H., Perron, G., Remedios, J., Ridolfi, M., Stiller, G., and Zander, R.: MIPAS: an instrument for atmospheric and climate research, *Atmos. Chem. Phys.*, 8, 2151–2188, doi:10.5194/acp-8-2151-2008, 2008.
- Fu, R., Hu, Y., Wright, J. S., Jiang, J. H., Dickinson, R. E., Chen, M., Filipiak, M., Read, W. G., Waters, J. W., and Wu, D. L.: Short circuit of water vapour and polluted air to the global stratosphere by convective transport over the Tibetan Plateau, *P. Natl. Acad. Sci. USA*, 103, 5664–5669, 2006.
- Galanter, M., Levy II, H., and Carmichael, G. R.: Impacts of biomass burning on tropospheric CO, NO<sub>x</sub>, and O<sub>3</sub>, *J. Geophys. Res.*, 105, 6633–6653, doi:10.1029/1999JD901113, 2000.
- Ganzeveld, L. and Lelieveld, J.: Dry deposition parameterization in a chemistry general circulation model and its influence on the distribution of reactive trace gases, *J. Geophys. Res.*, 100, 20999–21012, doi:10.1029/95JD02266, 1995.
- Gettelman, A., Salby, M. L., and Sassi, F.: Distribution and influence of convection in the tropical tropopause region, *J. Geophys. Res.*, 107, 4080, doi:10.1029/2001JD001048, 2002.
- Gettelman, A., Hoor, P., Pan, L. L., Randel, W. J., Heglin, M. I., and Birner, T.: The extratropical upper troposphere and lower stratosphere, *Rev. Geophys.*, 49, RG3003, doi:10.1029/2011RG000355, 2011.
- Glatthor, N., von Clarmann, T., Fischer, H., Funke, B., Grabowski, U., Höpfner, M., Kellmann, S., Kiefer, M., Linden, A., Milz, M., Steck, T., and Stiller, G. P.: Global peroxyacetyl nitrate (PAN) retrieval in the upper troposphere from limb emission spectra of the Michelson Interferometer for Passive Atmospheric Sounding (MIPAS), *Atmos. Chem. Phys.*, 7, 2775–2787, doi:10.5194/acp-7-2775-2007, 2007.
- Grewe, V., Brunner, D., Dameris, M., Grenfell, J. L., Hein, R., Shindell, D., and Staehelin, J.: Origin and Variability of Upper Tropospheric Nitrogen Oxides and Ozone at Northern Mid-Latitudes, *Atmos. Environ.*, 35, 3421–3433, 2001.
- Guenther, A., Karl, T., Harley, P., Wiedinmyer, C., Palmer, P. I., and Geron, C.: Estimates of global terrestrial isoprene emissions using MEGAN (Model of Emissions of Gases and Aerosols from Nature), *Atmos. Chem. Phys.*, 6, 3181–3210, doi:10.5194/acp-6-3181-2006, 2006.
- Harriss, R. C., Wofsy, S. C., Garstang, M., Browell, E. V., Molion, L. C. B., McNeal, R. J., Hoell Jr., J. M., Bendura, R. J., Beck, S. M., Navarro, R. L., Riley, J. T., and Snell R. L.: The Amazon boundary layer experiment (ABLE 2A) dry season 1985, *J. Geophys. Res.*, 93, 1351–1360, 1988.
- Harriss, R. C., Wofsy, S. C., Bartlett, D. S., Shipham, M. C., Jacob, D. J., Hoell Jr., J. M., Bendura, R. J., Drewry, J. W., McNeal, R. J., Navarro, R. L., Gidge, R. N., and Rabine, V. E.: The Arctic Boundary Layer Expedition (ABLE 3A): July–August 1988, *J. Geophys. Res.*, 97, 16383–16394, 1992.
- Harriss, R. C., Wofsy, S. C., Hoell Jr., J. M., Bendura, R. J., Drewry, J. W., McNeal, R. J., Pierce, D., Rabine, V., and Snell, R. L.: The Arctic Boundary Layer Expedition (ABLE-3B): July–August 1990, *J. Geophys. Res.*, 99, 1635–1643, 1994.
- Hoell Jr., J. M., Albritton, D. L., Gregory, G. L., McNeal, R. L., Beck, S. M., Bendura, R. J., and Drewry, J. W.: Operational overview of NASA GTE/CITE-2 airborne instrument intercomparison: Nitrogen dioxide, nitric acid, and peroxyacetyl nitrate, *J. Geophys. Res.*, 95, 10047–10054, 1990.
- Hoell Jr., J. M., Davis, D. D., Gregory, G. L., McNeal, R. J., Bendura, R. J., Drewry, J. W., Barrick, J. D., Kirchhoff, V. W. J. H., Motta, A. G., Navarro, R. L., Dorko, W. D., and Owen, D. W.: Operational overview of the NASA GTE/CITE-3 airborne instrument intercomparisons for sulfur dioxide, hydrogen sulfide, car-

- bonyl sulfide, dimethyl sulfide, and carbon disulfide, *J. Geophys. Res.*, 98, 23291–23304, doi:10.1029/93JD00453, 1993.
- Horowitz, L. W., Walters, S., Mauzerall, D. L., Emmons, L. K., Rasch, P. J., Granier, C., Tie, X., Lamarque, J., Schultz, M. G., Tyndall, G. S., Orlando, J. J., and Brasseur, G. P.: A global simulation of tropospheric ozone and related tracers, Description and evaluation of MOZART, version 2, *J. Geophys. Res.*, 108, 4784, doi:10.1029/2002JD002853, 2003.
- Hudman, R. C., Jacob, D. J., Cooper, O. R., Evans, M. J., Heald, C. L., Park, R. J., Fehsenfeld, F., Flocke, F., Holloway, J., Hübler, G., Kita, K., Koike, M., Kondo, Y., Neuman, A., Nowak, J., Oltmans, S., Parrish, D., Roberts, J. M., and Ryerson, T.: Ozone production in transpacific Asian pollution plumes and implications for ozone air quality in California, *J. Geophys. Res.*, 109, D23S10, doi:10.1029/2004jd004974, 2004.
- Hudman, R. C., Jacob, D. J., Turquety, S., Leibensperger, E. M., Murray, L. T., Wu, S., Gilliland, A. B., Avery, M., Bertram, T. H., Brune, W., Cohen, R. C., Dibb, J. E., Flocke, F. M., Fried, A., Holloway, J., Neuman, J. A., Orville, R., Perring, A., Ren, X., Ryerson, T. B., Sachse, G. W., Singh, H. B., Swanson, A., and Wooldridge, P. J.: Surface and lightning sources of nitrogen oxides in the United States: magnitudes, chemical evolution, and outflow, *J. Geophys. Res.*, 112, D12S05, doi:10.1029/2006JD007912, 2007.
- Keim, C., Liu, G. Y., Blom, C. E., Fischer, H., Gulde, T., Höpfner, M., Piesch, C., Ravagnani, F., Roiger, A., Schlager, H., and Sitnikov, N.: Vertical profile of peroxyacetyl nitrate (PAN) from MIPAS-STR measurements over Brazil in February 2005 and its contribution to tropical UT NO<sub>y</sub> partitioning, *Atmos. Chem. Phys.*, 8, 4891–4902, doi:10.5194/acp-8-4891-2008, 2008.
- Kettle, A. J. and Andreae, M. O.: Flux of Dimethylsulfide from the oceans: A comparison of updated data sets and flux models, *J. Geophys. Res.*, 105, 26793–26808, doi:10.1029/2000JD900252, 2000.
- Kulkarni J. R., Maheshkumar, R. S., Morwal, S. B., Padma kumari, B., Konwar, M., Deshpande, C. G., Joshi, R. R., Bhalwankar, R. V., Pandithurai, G., Safai, P. D., Narkhedkar, S. G., Dani, K. K., Nath, A., Nair, Sathy, Sapre, V. V., Puranik, P. V., Kandalgaonkar, S. S., Mujumdar, V. R., Khaladkar, R. M., Vijaykumar, R., Prabha, T. V., and Goswami, B. N.: The Cloud Aerosol Interaction and Precipitation Enhancement Experiment (CAIPEEX): overview and preliminary results (2012), *Curr. Sci.*, 102, 413–425, 2012.
- Labrador, L. J., von Kuhlmann, R., and Lawrence, M. G.: The effects of lightning-produced NO<sub>x</sub> and its vertical distribution on atmospheric chemistry: sensitivity simulations with MATCH-MPIC, *Atmos. Chem. Phys.*, 5, 1815–1834, doi:10.5194/acp-5-1815-2005, 2005.
- Lamsal, L. N., Martin, R. V., Padmanabhan, A., van Donkelaar, A., Zhang, Q., Sioris, C. E., Chance, K., Kurosu, T. P., and Newchurch, M. J.: Application of satellite observations for timely updates to global anthropogenic NO<sub>x</sub> emission inventories, *Geophys. Res. Lett.*, 38, L05810, doi:10.1029/2010GL046476, 2011.
- Li, Q., Jiang, J. H., Wu, D. L., Read, W. G., Livesey, N. J., Waters, J. W., Zhang, Y., Wang, B., Filipiak, M. J., Davis, C. P., Turquety, S., Wu, S., Park R. J., Yantosca R. M., and Jacob D. J.: Convective outflow of South Asian pollution: A global CTM simulation compared with EOS MLS observations, *Geophys. Res. Lett.*, 32, L14826, doi:10.1029/2005GL022762, 2005.
- Liang, Q., Rodriguez, J. M., Douglass, A. R., Crawford, J. H., Olson, J. R., Apel, E., Bian, H., Blake, D. R., Brune, W., Chin, M., Colarco, P. R., da Silva, A., Diskin, G. S., Duncan, B. N., Huey, L. G., Knapp, D. J., Montzka, D. D., Nielsen, J. E., Pawson, S., Riemer, D. D., Weinheimer, A. J., and Wisthaler, A.: Reactive nitrogen, ozone and ozone production in the Arctic troposphere and the impact of stratosphere-troposphere exchange, *Atmos. Chem. Phys.*, 11, 13181–13199, doi:10.5194/acp-11-13181-2011, 2011.
- Liu, C. and Zipser E. J.: Global distribution of convection penetrating the tropical tropopause, *J. Geophys. Res.*, 110, D23104, doi:10.1029/2005JD006063, 2005.
- Martin, R. V., Sauvage, B., Folkins, I., Sioris, C. E., Boone, C., Bernath, P., and Ziemke, J.: Space-based constraints on the production of nitric oxide by lightning, *J. Geophys. Res.*, 112, D09309, doi:10.1029/2006JD007831, 2007.
- Miyazaki, K., Eskes, H. J., and Sudo, K.: Global NO<sub>x</sub> emission estimates derived from an assimilation of OMI tropospheric NO<sub>2</sub> columns, *Atmos. Chem. Phys.*, 12, 2263–2288, doi:10.5194/acp-12-2263-2012, 2012.
- Murray, L. T., Jacob, D. J., Logan, J. A., Hudman, R. C., and Koshak, W. J.: Optimized regional and interannual variability of lightning in a global chemical transport model constrained by LIS/OTD satellite data, *J. Geophys. Res.*, 117, D20307, doi:10.1029/2012JD017934, 2012.
- Nightingale, P. D., Malin, G., Law, C. S., Watson, A. J., Liss, P. S., Liddicoat, M. I., Boutin, J., and Upstill-Goddard, R. C.: In situ evaluation of air-sea gas exchange parameterizations using novel conservative and volatile tracers, *Global Biogeochem. Cycles*, 14, 373–387, doi:10.1029/1999GB900091, 2000.
- O'Sullivan, D. W., Heikes, B. G., Lee, M., Chang, W., Gregory, G. L., Blake, D. R., and Sachs, G. W.: Distribution of hydrogen peroxide and methylhydroperoxide over the Pacific and South Atlantic Oceans, *J. Geophys. Res.*, 104, 5635–5646, 1999.
- Park, M., Randel, W. J., Kinnison, D. E., Garcia, R. R., and Choi, W.: Seasonal variation of methane, water vapour, and nitrogen oxides near the tropopause: Satellite observations and model simulations, *J. Geophys. Res.*, 109, D03302, doi:10.1029/2003JD003706, 2004.
- Park, M., Randel, W. J., Gettleman, A., Massie, S. T., and Jiang, J. H.: Transport above the Asian summer monsoon anticyclone inferred from Aura Microwave Limb Sounder tracers, *J. Geophys. Res.*, 112, D16309, doi:10.1029/2006JD008294, 2007.
- Park, M., Randel, W. J., Emmons, L. K., and Livesey, N. J.: Transport pathways of carbon monoxide in the Asian summer monsoon diagnosed from Model of Ozone and Related Tracers (MOZART), *J. Geophys. Res.*, 114, D08303, doi:10.1029/2008JD010621, 2009.
- Penki, R. K. and Kamra, A. K.: Lightning distribution with respect to the monsoon trough position during the Indian summer monsoon season, *J. Geophys. Res.*, 118, 4780–4787, doi:10.1002/jgrd.50382, 2013.
- Pham, M., Muller, J. F., Brasseur, G. P., Granier, C., and Megie, G.: A three-dimensional study of the tropospheric sulfur cycle, *J. Geophys. Res.*, 100, 26061–26092, doi:10.1029/95JD02095, 1995.
- Pozzoli, L., Bey, I., Rast, J. S., Schultz, M. G., Stier, P., and Feichter, J.: Trace gas and aerosol interactions in the

- fully coupled model of aerosol-chemistry-climate ECHAM5-HAMMOZ: 1. Model description and insights from the spring 2001 TRACE-P experiment, *J. Geophys. Res.*, 113, D07308, doi:10.1029/2007JD009007, 2008a.
- Pozzoli, L., Bey, I., Rast, J. S., Schultz, M. G., Stier, P., and Feichter, J.: Trace gas and aerosol interactions in the fully coupled model of aerosol-chemistry-climate ECHAM5-HAMMOZ: 2. Impact of heterogeneous chemistry on the global aerosol distributions, *J. Geophys. Res.*, 113, D07309, doi:10.1029/2007JD009008, 2008b.
- Pozzoli, L., Janssens-Maenhout, G., Diehl, T., Bey, I., Schultz, M. G., Feichter, J., Vignati, E., and Dentener, F.: Re-analysis of tropospheric sulfate aerosol and ozone for the period 1980–2005 using the aerosol-chemistry-climate model ECHAM5-HAMMOZ, *Atmos. Chem. Phys.*, 11, 9563–9594, doi:10.5194/acp-11-9563-2011, 2011.
- Prabha, T. V., Khain, A., Maheshkumar, R. S., Pandithurai, G., Kulkarni, J. R., and Goswami, B. N.: Microphysics of premonsoon and monsoon clouds as seen from in situ measurements during the Cloud Aerosol Interaction and Precipitation Enhancement Experiment (CAIPEEX), *J. Atmos. Sci.*, 68, 1882–1901, doi:10.1175/2011JAS3707.1, 2011.
- Ranalkar, M. R. and Chaudhari, H. S.: Seasonal variation of lightning activity over the Indian subcontinent, *Meteorol. Atmos. Phys.*, 104, 125–134, 2009.
- Randel, W. J. and Park, M.: Deep convective influence on the Asian summer monsoon anticyclone and associated tracer variability observed with Atmospheric Infrared Sounder (AIRS), *J. Geophys. Res.*, 111, D12314, doi:10.1029/2005JD006490, 2006.
- Randel, W. J., Park, M., Emmons, L., Kinnison, D., Bernath, P., Walker, K. A., Boone, C., and Pumphrey, H.: Asian monsoon transport of pollution to the stratosphere, *Science*, 328, 611–613, 2010.
- Real, E., Orlandi, E., Law, K. S., Fierli, F., Josset, D., Cairo, F., Schlager, H., Borrmann, S., Kunkel, D., Volk, C. M., McQuaid, J. B., Stewart, D. J., Lee, J., Lewis, A. C., Hopkins, J. R., Ravagnani, F., Ulanovski, A., and Lioussse, C.: Cross-hemispheric transport of central African biomass burning pollutants: implications for downwind ozone production, *Atmos. Chem. Phys.*, 10, 3027–3046, doi:10.5194/acp-10-3027-2010, 2010.
- Ridley, B. A., Madronich, S., Chatfield, R. B., Walega, J. G., Shetter, R. E., Carroll, M. A., and Montzka D. D.: Measurements and model simulations of the photostationary state during the Mauna Loa Observatory Photochemistry Experiment: Implications for radical concentrations and ozone production and loss rates, *J. Geophys. Res.*, 97, 10375–10388, doi:10.1029/91JD02287, 1992.
- Ridley, B. A., Walega, J. G., Dye, J. E., and Grahek, F. E.: Distributions of NO, NO<sub>x</sub>, NO<sub>y</sub>, and O<sub>3</sub> to 12 km altitude during the summer monsoon season over New Mexico, *J. Geophys. Res.*, 99, 25519–25534, 1994.
- Roeckner, E., Bauml, G., Bonaventura, L., Brokopf, R., Esch, M., Giorgetta, M., Hagemann, S., Kirchner, I., Kornblueh, L., Manzini, E., Rhodin, A., Schlese, U., Schulzweida, U., and Tompkins, A.: The atmospheric general circulation model ECHAM5: Part 1, Tech. Rep. 349, Max Planck Institute for Meteorology, Hamburg, ISSN: 0937–1060, 2003.
- Sander, S. P., Friedl, R. R., Ravishankara, A. R., Golden, D. M., Kolb, C. E., Kurylo, M. J., Huie, R. E., Orkin, V. L., Molina, M. J., Moortgat, G. K., and Finlayson-Pitts, B. J.: Chemical kinetics and photochemical data for use in atmospheric studies, evaluation number 14, JPL Publ. 02–25, Jet Propul. Lab., Calif. Inst. of Technol., Pasadena, available at: [http://jpldataeval.jpl.nasa.gov/pdf/JPL\\_02-25\\_rev02.pdf](http://jpldataeval.jpl.nasa.gov/pdf/JPL_02-25_rev02.pdf) (last access: 10 October 2015), 2003.
- Schmitz, J. T. and Mullen, S. L.: Water vapor transport associated with the summertime North American Monsoon as depicted by ECMWF analyses, *J. Climate*, 9, 1621–1634, 1996.
- Schulz, M., de Leeuw, G., and Balkanski, Y.: Sea salt aerosol source functions and emissions, in: Emission of atmospheric trace compounds, Volume 18 of the series Advances in Global Change Research, edited by: Granier, C., Artaxo, P., and Reeves, C., Springer, the Netherlands, 333–359, 2004.
- Schultz, M., Backman, L., Balkanski, Y., Bjoerndalsaeter, S., Brand, R., Burrows, J., Dalsoeren, S., de Vasconcelos, M., Grodtmann, B., Hauglustaine, D., Heil, A., Hoelzemann, J., Isaksen, I., Kaurola, J., Knorr, W., Ladstaetter-Weienmayer, A., Mota, B., Oom, D., Pacyna, J., Panasiuk, D., Pereira, J., Pulles, T., Pyle, J., Rast, S., Richter, A., Savage, N., Schnadt, C., Schulz, M., Spessa, A., Staehelin, J., Sundet, J., Szopa, S., Thonicke, K., van het Bolscher, M., van Noije, T., van Velthoven, P., Vik, A., and Wittrock, F.: REanalysis of the TROpospheric chemical composition over the past 40 years (RETRO). A long-term global modeling study of tropospheric chemistry. Final Report, Tech. rep., Max Planck Institute for Meteorology, Hamburg, Germany, 2007.
- Schultz, M. G., Heil, A., Hoelzemann, J. J., Spessa, A., Thonicke, K., Goldammer, J. G., Held, A. C., Pereira, J. M. C., and van het Bolscher, M.: Global wildland fire emissions from 1960 to 2000, *Global Biogeochem. Cy.*, 22, GB2002, doi:10.1029/2007GB003031, 2008.
- Schumann, U. and Huntrieser, H.: The global lightning-induced nitrogen oxides source, *Atmos. Chem. Phys.*, 7, 3823–3907, doi:10.5194/acp-7-3823-2007, 2007.
- Shepon, A., Gildor, H., Labrador, L. J., Butler, T., Ganzeveld, L. N., and Lawrence, M. G.: Global reactive nitrogen deposition from lightning NO<sub>x</sub>, *J. Geophys. Res.*, 112, D06304, doi:10.1029/2006JD007458, 2007.
- Singh, H. B.: Reactive nitrogen in the troposphere, *Environ. Sci. Technol.*, 21, 320–327, 1987.
- Singh, H. B., Salas, L. J., and Viezee, W.: Global distribution of peroxyacetyl nitrate, *Nature*, 321, 588–591, 1986.
- Singh, H. B., Viezee, W., Chen, Y., Thakur, A. N., Kondo, Y. and Talbot, R. W., Gregory, G. L., Sachse, G. W., Blake, D. R., Bradshaw, J. D., Wang, Y., and Jacob D. J.: Latitudinal distribution of reactive nitrogen in the free troposphere over the Pacific Ocean in late winter/early spring, *J. Geophys. Res.*, 103, 28237–28246, doi:10.1029/98JD01891, 1998.
- Singh, H. B., Brune, W. H., Crawford, J. H., Jacob, D. J., and Russell, P. B.: Overview of the summer 2004 Intercontinental Chemical Transport Experiment – North America (INTEX-A), *J. Geophys. Res.*, 111, D24S01, doi:10.1029/2006JD007905, 2006.
- Stier, P., Feichter, J., Kinne, S., Kloster, S., Vignati, E., Wilson, J., Ganzeveld, L., Tegen, I., Werner, M., Balkanski, Y., Schulz, M., Boucher, O., Minikin, A., and Petzold, A.: The aerosol-climate model ECHAM5-HAM, *Atmos. Chem. Phys.*, 5, 1125–1156, doi:10.5194/acp-5-1125-2005, 2005.
- Talbot, R. W., Dibb, J. E., Scheuer, E. M., Bradshaw, J. D., Sandholm, S. T., Singh, H. B., Blake, D. R., Blake, N. J., Atlas, E.,

- and Flocke, F.: Tropospheric reactive odd nitrogen over the South Pacific in austral springtime, *J. Geophys. Res.*, 105, 6681–6694, doi:10.1029/1999JD901114, 2000.
- Talukdar, R. K., Burkholder, J. B., Schmoltner, A., Roberts, J. M., Wilson, R. R., and Ravishankara, A. R.: Investigation of loss processes for peroxyacetyl nitrate in the atmosphere: UV photolysis and reaction with OH, *J. Geophys. Res.*, 100, 14163–14173, 1995.
- Tang, J. H., Chan, L. Y., Chang, C. C., Liu, S., and Li, Y. S.: Characteristics and sources of non-methane hydrocarbons in background atmospheres of eastern, southwestern, and southern China, *J. Geophys. Res.*, 114, D03304, doi:10.1029/2008JD010333, 2009.
- Tegen, I., Harrison, S. P., Kohfeld, K., Prentice, I. C., Coe, M., and Heimann, M.: Impact of vegetation and preferential source areas on global dust aerosol: Results from a model study, *J. Geophys. Res.*, 107, 4576, doi:10.1029/2001JD000963, 2002.
- Tereszczuk, K. A., Moore, D. P., Harrison, J. J., Boone, C. D., Park, M., Remedios, J. J., Randel, W. J., and Bernath, P. F.: Observations of peroxyacetyl nitrate (PAN) in the upper troposphere by the Atmospheric Chemistry Experiment-Fourier Transform Spectrometer (ACE-FTS), *Atmos. Chem. Phys.*, 13, 5601–5613, doi:10.5194/acp-13-5601-2013, 2013.
- Tie, X. X., Zhang, R., Brasseur, G., Emmons, L., and Lei, W.: Effects of lightning on reactive nitrogen and nitrogen reservoir species in the troposphere, *J. Geophys. Res.-Atmos.*, 106, 3167–3178, doi:10.1029/2000JD900565, 2001.
- Uppala, S. M., Kållberg, P. W., Simmons, A. J., Andrae, U., Costa, Bechtold V. Da, Fiorino, M., Gibson, J. K., Haseler, J., Hernandez, A., Kelly, G. A., Li, X., Onogi, K., Saarinen, S., Sokka, N., Allan, R. P., Andersson, E., Arpe, K., Balmaseda, M. A., Beljaars, A. C. M., Berg, L., Van De, Bidlot, J., Bormann, N., Cairnes, S., Chevallier, F., Dethof, A., Dragosavac, M., Fisher, M., Fuentes, M., Hagemann, S., Hólm, E., Hoskins, B. J., Isaksen, I., Janssen, P. A. E. M., Jenne, R., McNally, A. P., Mahfouf, J.-F., Morcrette, J.-J., Rayner, N. A., Saunders, R. W., Simon, P., Sterl, A., Trenberth, K. E., Untch, A., Vasiljevic, D., Viterbo, P., and Woollen, J.: The ERA-40 re-analysis, *Q. J. Roy. Meteorol. Soc.*, 131, 2961–3012, doi:10.1256/qj.04.176, 2005.
- von Clarmann, T., Höpfner, M., Kellmann, S., Linden, A., Chauhan, S., Funke, B., Grabowski, U., Glatthor, N., Kiefer, M., Schieferdecker, T., Stiller, G. P., and Versick, S.: Retrieval of temperature, H<sub>2</sub>O, O<sub>3</sub>, HNO<sub>3</sub>, CH<sub>4</sub>, N<sub>2</sub>O, ClONO<sub>2</sub> and ClO from MIPAS reduced resolution nominal mode limb emission measurements, *Atmos. Meas. Tech.*, 2, 159–175, doi:10.5194/amt-2-159-2009, 2009.
- Wiegele, A., Glatthor, N., Höpfner, M., Grabowski, U., Kellmann, S., Linden, A., Stiller, G., and von Clarmann, T.: Global distributions of C<sub>2</sub>H<sub>6</sub>, C<sub>2</sub>H<sub>2</sub>, HCN, and PAN retrieved from MIPAS reduced spectral resolution measurements, *Atmos. Meas. Tech.*, 5, 723–734, doi:10.5194/amt-5-723-2012, 2012.
- Xiong, X., Houweling, S., Wei, J., Maddy, E., Sun, F., and Barnet, C.: Methane plume over south Asia during the monsoon season: satellite observation and model simulation, *Atmos. Chem. Phys.*, 9, 783–794, doi:10.5194/acp-9-783-2009, 2009.
- Zhang, L., Jacob, D. J., Boersma, K. F., Jaffe, D. A., Olson, J. R., Bowman, K. W., Worden, J. R., Thompson, A. M., Avery, M. A., Cohen, R. C., Dibb, J. E., Flock, F. M., Fuelberg, H. E., Huey, L. G., McMillan, W. W., Singh, H. B., and Weinheimer, A. J.: Transpacific transport of ozone pollution and the effect of recent Asian emission increases on air quality in North America: an integrated analysis using satellite, aircraft, ozonesonde, and surface observations, *Atmos. Chem. Phys.*, 8, 6117–6136, doi:10.5194/acp-8-6117-2008, 2008.
- Zhao, C., Wang, Y., Choi, Y., and Zeng, T.: Summertime impact of convective transport and lightning NO<sub>x</sub> production over North America: modeling dependence on meteorological simulations, *Atmos. Chem. Phys.*, 9, 4315–4327, doi:10.5194/acp-9-4315-2009, 2009.
- Ziereis, H., Schlager, H., Schulte, P., van Velthoven, P. F. J., and Slemr, F.: Distributions of NO, NO<sub>x</sub>, and NO<sub>y</sub> in the upper troposphere and lower stratosphere between 28° N and 61° N during POLINAT 2, *J. Geophys. Res.*, 105, 3653–3664, doi:10.1029/1999JD900870, 2000.